

Toward neurobiological characterization of functional homogeneity in the human cortex: regional variation, morphological association and functional covariance network organization

Lili Jiang · Ting Xu · Ye He · Xiao-Hui Hou ·
Jinhui Wang · Xiao-Yan Cao · Gao-Xia Wei ·
Zhi Yang · Yong He · Xi-Nian Zuo

Received: 20 November 2013 / Accepted: 11 May 2014 / Published online: 6 June 2014
© Springer-Verlag Berlin Heidelberg 2014

Abstract Local functional homogeneity of the human cortex indicates the boundaries between functionally heterogeneous regions and varies remarkably across the cortical mantle. It is unclear whether these variations have the neurobiological and structural basis. We employed structural and resting-state functional magnetic resonance imaging scans from 482 healthy subjects and computed the vertex-wise regional homogeneity of low-frequency fluctuations (2dReHo) and five measures of cortical morphology. We then used these metrics to examine regional variation, morphological association and functional

covariance network of 2dReHo. Within the ventral visual stream, increases of 2dReHo reflect reduced complexity of information processing or functional hierarchies. Along the divisions of the prefrontal cortex and posteromedial cortex, the gradients of 2dReHo revealed the hierarchical organization within the two association areas, respectively. Individual differences in 2dReHo are associated with those of cortical morphology, and their whole-brain inter-regional covariation is organized into a functional covariance network, comprising five hierarchically organized modules with hubs of both primary sensory and high-order association areas. These highly reproducible observations suggest that local functional homogeneity has neurobiological relevance that is likely determined by anatomical, developmental and neurocognitive factors and should serve as a neuroimaging marker to investigate the human brain function.

L. Jiang · T. Xu · Y. He · X.-H. Hou · X.-Y. Cao · G.-X. Wei ·
Z. Yang · X.-N. Zuo (✉)
Laboratory for Functional Connectome and Development, Key
Laboratory of Behavioral Science and Magnetic Resonance
Imaging Research Center, Institute of Psychology, Chinese
Academy of Sciences, Room 708, Southern Building,
No. 16 Lincui Road, Chaoyang District, Beijing 100101, China
e-mail: zuoxn@psych.ac.cn
URL: <http://lfc.d.psych.ac.cn>

Y. He · X.-H. Hou
University of Chinese Academy of Sciences, Beijing 100049,
China

J. Wang · X.-Y. Cao
Center for Cognition and Brain Disorders and the Affiliated
Hospital, Hangzhou Normal University, Hangzhou,
Zhejiang 310036, China

Y. He
State Key Laboratory of Cognitive Neuroscience and Learning
and International Data Group/McGovern Institute for Brain
Research, Beijing Normal University, Beijing 100087, China

Y. He · X.-N. Zuo
Center for Collaboration and Innovation in Brain and Learning
Sciences, Beijing Normal University, Beijing 100087, China

Keywords Functional homogeneity · Prefrontal cortex ·
Posteromedial cortex · Functional hierarchy · Structural
morphometry · Functional covariance · Network

Introduction

Functional connectomics has become an increasingly powerful tool for characterizing human brain function (Biswal et al. 2010; Zuo et al. 2012; Craddock et al. 2013). Although previous studies have extensively investigated the intrinsic functional connectivity among distant regions using resting-state functional magnetic resonance imaging (fMRI), the regional homogeneity of local functional activity (i.e., functional homogeneity) has been overlooked for some time (Biswal et al. 1995; Kelly et al. 2012). Observations of the structural basis of functional

connectivity performed using computational simulations have indicated the potential roles of local functional homogeneity and of its regional variation (Sporns et al. 2005; Deco et al. 2009, 2010; Honey et al. 2009; Breakspear et al. 2010). In this study, we aim to justify local functional homogeneity as a biologically meaningful measure for exploring human brain connectomics by examining its regional variation, morphological correlates and covariance network organization.

Local functional homogeneity of the human cortex indicates the boundaries between functionally heterogeneous regions. Although the whole-brain functional homogeneity has been mapped in previous studies (Zang et al. 2004; He et al. 2007a; Long et al. 2008; Tomasi and Volkow 2010) and is highly test–retest reliable (Zuo et al. 2013; Zuo and Xing 2014), its regional variation and robustness across individuals have never been systematically investigated. The homogeneity of cell number/type and neuron density most likely contributes to functional homogeneity within a small region (Lichtman and Denk 2011); thus, this regional variation in micro-level homogeneity could also contribute to the regional variation in local functional homogeneity. Regarding brain connectomics, although previous large-scale functional connectomes studies have provided great insights into brain network organization (Bullmore and Sporns 2009, 2012), regional variations in local functional homogeneity have suggested that defining a node based on a large structural region and building an edge in a functional connectivity graph can be problematic. Simply averaging the voxel-wise time series in a large region ignores the fact that the strength of functional homogeneity within large structural areas is typically low and highly variable across spatial locations, leading to difficulties in interpreting the mean time series and derived connectome metrics. A promising solution to this problem is to parcellate the brain into a set of functionally homogeneous regions (i.e., functional parcellation) at both the groups (Bellec et al. 2010; Yeo et al. 2011; Craddock et al. 2012; Zuo et al. 2012) and individual levels (Blumensath et al. 2013; Wig et al. 2013). For this purpose, a comprehensive map of local functional homogeneity across the human cortex, particularly its regional variations, is essential.

The regional variation in local functional homogeneity within a brain circuit or region can help provide insight into the intrinsic architecture of the human brain function. The ventral visual stream (VVS) is one of the two widely accepted and influential models of the neural processing of the visual circuit in both nonhuman primates and humans. The VVS has a clear hierarchical organization (Ungerleider and Haxby 1994). Identifying the relation between the regional homogeneity and the information processing hierarchy in this stream would begin to clarify neurobiological and cognitive roles of local functional homogeneity.

The prefrontal cortex (PFC) is related to all higher brain functions, including affect, social behavior, and cognitive control (see Amodio and Frith 2006; Wood and Grafman 2003; Miller et al. 2000 for reviews). These previous studies have proposed several unifying theories of PFC function; however, the functional organization of the PFC is currently under much debate. Existing parcellation paradigms of the PFC have primarily been generated for the macaque based on stained cell bodies and/or fiber patterns. RFMRI has recently improved this situation and gained new insights into the functional anatomy of macaque PFC (Hutchison and Everling 2013). This technology has also accelerated the recent advances concerning functional parcellation of the human brain (e.g., Yeo et al. 2011). Examining the regional variation in the local functional homogeneity of common functional connectivity networks that overlap with the human PFC will greatly enrich the current knowledge of the PFC's functional hierarchy.

The posteromedial cortex (PMC) has been less accurately mapped with its brain connectivity profile using traditional brain mapping technologies because the PMC is hidden in a deep anatomical location and is rarely hurt under various traumatic brain injury conditions. Recent RFMRI studies have revealed that the highest functional homogeneity (hot spots) appeared in the (PMC) (He et al. 2007a; Long et al. 2008; Tomasi and Volkow 2010; Zuo et al. 2013) across the cerebral cortex. This finding might be an indication of the previous observation that this unique and mysterious high-order association area in the human brain exhibits the highest resting metabolic rates (Raichle et al. 2001) and network centrality of information flow (Hagmann et al. 2008; Buckner et al. 2009; He et al. 2009; Zuo et al. 2012). Long-distance connectivity with different portions of the PMC has been increasingly investigated within both healthy and clinical populations (see Cavanna and Trimble 2006; Leech and Sharp 2014 for reviews). Surprisingly, regional variation in local functional connectivity within the PMC has rarely been examined although this variation has great potential insights into the PMC's functional anatomy. We will systematically investigate the regional variation in 2dReHo within the VVS, PFC and within the PMC.

Although individual differences in distant functional connectivity have been demonstrated with its biologically meaningful indication of brain morphology (Mueller et al. 2013; Alexander-Bloch et al. 2013), the individual variability of 2dReHo and its morphological association have rarely been examined. The inter-regional covariation in brain morphological measurements (i.e., structural covariance) across individuals has been proposed to reflect the synchronization of development processes between two regions (Mechelli et al. 2005; Alexander-Bloch and Giedd 2013). Mapping the structure covariance networks has been

Table 1 MRI information across three imaging sites

	Beijing enhanced	Cambridge	NKI Rockland
Scanner			
Manufacturer	Siemens	Siemens	Siemens
Magnet	3.0 Tesla	3.0 Tesla	3.0 Tesla
System	TrioTim B15	TrioTim B15	TrioTim B15
MP-RAGE			
TR	2,530 ms	2,200 ms	2,500 ms
TE	3.39 ms	1.04–7.01 ms ^a	3.50 ms
TI	1,100 ms	1,100 ms	1,200 ms
FA	7°	7°	8°
FoV	256 mm	230 mm	256 mm
#Slices	128	144	192
Voxel size	1.3 × 1.0 × 1.0 mm	1.2 × 1.2 × 1.2 mm	1.0 × 1.0 × 1.0 mm
EPI			
TR	2,000 ms	3,000 ms	2,500 ms
TE	30 ms	30 ms	30 ms
FA	90°	85°	80°
FoV	200 mm	216 mm	216 mm
#Slices	33	47	38
Voxel size	3.1 × 3.1 × 3.6 mm	3.0 × 3.0 × 3.0 mm	3.0 × 3.0 × 3.3 mm
#Time points	240	124	260

Repetition time (TR), Echo Time (TE), Inversion Time (TI), Flip Angle (FA), Field of View (FoV)

^a A multiecho (four different TEs) MP-RAGE sequence was used to increase image contrast through weighted averaging of the four derived images

increasingly applied to study the brain's topological organization (He et al. 2007b; Zhang et al. 2011), development/aging (Zielinski et al. 2010; Montembeault et al. 2012; Li et al. 2013), behavior/cognition (Kanai and Rees 2011; Bernhardt et al. 2013) and disease (Zielinski et al. 2012; Liao et al. 2013). A comprehensive assessment on 2dReHo's correlates of various brain morphological metrics, which are based on its individual differences and on its inter-regional functional covariance, can offer a unique opportunity for mapping the human brain's functional organization at both local spatial scale (millimeters) and long temporal scale (years), as well as its structural basis.

This study used a large sample ($N = 482$) of multimodal imaging datasets of the human brain to examine the regional variation in local functional homogeneity within the ventral visual stream, the PFC and within the PMC. We also investigated the inter-regional covariation in local functional homogeneity by mapping the derived functional covariance network and its network properties such as centrality and modules. To directly examine the morphological association of local functional homogeneity, we conducted a correlational analysis between local functional homogeneity and cortical morphology across the cerebral cortex. The findings presented in this study are highly reproducible across three imaging sites and reliable across a 2-day test–retest occasion. These results suggest that local functional homogeneity has neurobiological relevance that is likely determined by cognitive, structural, and by developmental factors.

Materials and methods

Participants and magnetic resonance imaging

A total of 504 healthy participants were scanned at three different sites using Siemens MAGNETOM TrioTim 3T scanners: (1) Beijing Enhanced ($N = 180$) (Yan et al. 2011), (2) Cambridge ($N = 198$) (Yeo et al. 2011), and (3) Nathan Kline Institute (NKI)/Rockland ($N = 126$) (Nooner et al. 2012; Yang et al. 2014; Cao et al. 2014). Details of MRI information for the three imaging sites are summarized in Table 1. As an open science effort, these datasets have been made publicly available via the 1000 Functional Connectomes Project (FCP¹: Biswal et al. 2010) and the International Data-sharing Initiative (INDI²: Milham 2012).

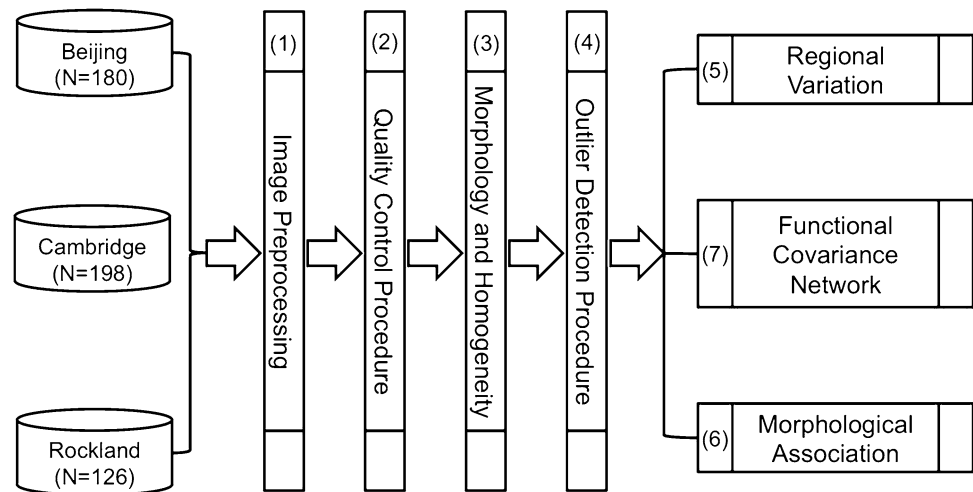
To minimize MRI spatial distortion and signal loss (especially in the orbital frontal cortex of the PFC) as well as achieve a higher temporospatial resolution in exploring the functional hierarchy of the PFC, we employed another public RFMRI dataset from the Human Connectome Project (HCP³) (Van Essen et al. 2013). These data were acquired with advanced multi-band RFMRI sequences from 80 unrelated healthy participants in the HCP Q3 release database. Each HCP subject underwent 1 h of

¹ http://fcon_1000.projects.nitrc.org/fcpClassic/FcpTable.html.

² http://fcon_1000.projects.nitrc.org/indi/pro/nki.html.

³ <http://www.humanconnectome.org>.

Fig. 1 Flowchart of the overall analytic strategy and computational pipeline



whole-brain RFMRI scanning acquired with two pairs of 15-min runs in 2 days and thus had four 15-min RFMRI scans (rfMRI_REST1_LR, rfMRI_REST1_RL, rfMRI_REST2_LR, rfMRI_REST2_RL). A spatial resolution of 2-mm voxel and a temporal resolution of 0.7 s were achieved with a multi-band EPI acceleration factor of 8 (Moeller et al. 2010; Feinberg et al. 2010). All subjects were instructed to lie with their eyes open, with “relaxed” fixation on a white cross (on a dark background), think of nothing in particular, and not fall asleep. More details of these data can be found in HCP Q3 release reference manual.⁴

Overall analytic strategy

Figure 1 illustrates the following overall analytic strategy: (1) first, individual structural and functional images are preprocessed, followed by (2) a quality control procedure (QCP) to exclude data with severe problems (e.g., incomplete scan, head motion, or bad registration). (3) For all data passing the QCP, metrics of both brain functional homogeneity and structural morphology are computed vertex-wise on the cortical mantle. (4) Using these metrics, an outlier detection procedure (ODP) is developed to further exclude participants from subsequent group-level analyses. All computational procedures are performed on the Dell Blade Cluster System at the Institute of Psychology, Chinese Academy of Sciences. Finally, we conduct three types of functional homogeneity analyses at the group level to systematically investigate the (5) regional variation, (6) morphological association, and (7) functional covariance network of local functional homogeneity in the human brain.

Image preprocessing

For each participant, all MRI images were preprocessed using the Connectome Computation System (CCS).⁵ The CCS was developed based on FCP scripts⁶ and extends the functionality onto the cortical surface by integrating AFNI (Cox 2012), FSL (Jenkinson et al. 2012) and FreeSurfer (Fischl 2012) software with shell and MATLAB scripts. The CCS combines anatomical, structural and functional information to provide a computational platform for brain connectome analysis with multi-modal neuroimaging data. The data preprocessing was composed of steps for both anatomical and functional processing.

The structural image processing included the following steps of brain cortical surface reconstruction (Dale et al. 1999; Fischl et al. 1999; Segonne et al. 2004, 2007): (1) MR image noise removal using a spatially adaptive non-local means filter (Xing et al. 2011; Zuo and Xing 2011) and MR intensity inhomogeneity correction; (2) brain extraction using a hybrid watershed/surface deformation procedure; (3) automated segmentation of the cerebrospinal fluid (CSF), white matter (WM) and deep gray matter (GM) volumetric structures; (4) generation of cutting planes to disconnect the two hemispheres and subcortical structures; (5) repair of the interior holes of the segmentation; (6) a triangular mesh tessellation and the mesh deformation over the GM-WM boundary to produce a smooth representation of the GM-WM interface (white surface) and of the GM-CSF interface (pial surface); (7) topological defect correction on the surface, (8) individual surface mesh inflation into a sphere; and (9) estimation of the deformation between the resulting spherical mesh and a

⁴ <http://www.humanconnectome.org/documentation/Q3>.

⁵ <http://fcd.psych.ac.cn/ccs.html>.

⁶ <http://www.nitrc.org/frs/downloadlink.php/2628>.

common spherical coordinate system that aligned the cortical folding patterns across subjects.

The functional image preprocessing involved the following processes: (1) removing the first 5 EPI volumes from each scan to allow for signal equilibration; (2) despiking time series with an hyperbolic tangent function to detect and reduce outliers (spikes); (3) slice timing using Fourier interpolation to temporally correct the interleaved slice acquisition; (4) aligning each volume to a “base” image (the mean EPI image) using Fourier interpolation to correct the between-head movements; (5) normalizing the 4D global mean intensity to 10,000 to allow inter-subject comparisons; (6) regressing out the WM/CSF mean time series and the Friston-24 motion time series to reduce the effects of these confounding factors (Zuo et al. 2013; Yan et al. 2013a); (7) filtering the residual time series with a band-pass (0.01–0.1 Hz) to extract the low-frequency fluctuations; (8) removing both linear and quadratic trends; and (9) aligning individual motion corrected functional images to the individual anatomical image using the GM-WM boundary-based registration (BBR) algorithm (Greve and Fischl 2009).

Using the combination of BBR deformation and spherical surface normalization, first, the individually preprocessed 4D RFMRI time series were projected onto the *fsaverage* standard cortical surface with 163,842 vertices per hemisphere apart from 1 mm neighboring pairs of vertices on average. Then, the data were down-sampled onto the *fsaverage5* standard cortical surface (3.8-mm neighboring-vertex distance), which contained 10,242 vertices per hemisphere (Yeo et al. 2011).

The HCP datasets underwent the HCP preprocessing pipeline (Smith et al. 2013; Glasser et al. 2013). Similar to the CCS, this pipeline puts significant effort into obtaining an accurate registration of the RFMRI images to the high-resolution (0.7-mm isotropic voxel) structural image of each subject. This accurate registration allows the transformation of the cortical RFMRI signal from the originally acquired 3D voxel matrix onto a gray matter surface mesh. Surface-based analysis represents gray matter with greater respect to its natural geometry and therefore allows for better functional alignment across subjects (Van Essen and Dierker 2007) and reliability improvements (Zuo et al. 2013). The minimally preprocessed individual RFMRI time series were transferred from native surface meshes to the Conte69 32 k template mesh (2-mm average vertex spacing, with 32,494 vertices per hemisphere) (Van Essen et al. 2012) and further smoothed (2-mm FWHM) on the surface (Smith et al. 2013). Several efforts have also been made to address various noisy confounds in these RFMRI data. A minimal high-pass filtering with a 2000-s FWHM was applied, which was similar to the removal of linear trends from the data. The 24 confound time series derived

from the motion estimation were also regressed out of the data (Yan et al. 2013a; Satterthwaite et al. 2013). FIX (FMRIB’s ICA-based X-noiseifier) was applied to classify RFMRI data components in the volume space into “good” versus “bad” (Salimi-Khorshidi et al. 2014; Griffanti et al. 2014). Then, bad components identified as artifactual processes by FIX were removed from the RFMRI data in the surface space.

Quality control procedure

Following the preprocessing steps of individual images, the CCS provides a quality control procedure (QCP) to ensure the quality of processed images. Specifically, this procedure produces basic information concerning preprocessed images including screenshots for visual inspection of: (1) brain extraction or skull stripping, (2) brain tissue segmentation, (3) pial and white surface reconstruction, (4) BBR-based functional image registration, and (5) head motion during RFMRI, and several quantities, including the following: (1) the maximum distance of translational head movement (maxTran), (2) the maximum degree of rotational head movement (maxRot), (3) the mean frame-wise displacement (meanFD) (Power et al. 2012; Patriat et al. 2013), and (4) the minimal cost of the BBR co-registration (mcBBR). All subjects with bad brain extraction, tissue segmentation and with bad surface construction will be excluded from the subsequent analysis. In addition, all datasets entering the subsequent analysis must meet the following criteria: (1) $\text{maxTran} \leq 2$ mm, (2) $\text{maxRot} \leq 2^\circ$, (3) $\text{meanFD} \leq 0.2$ mm, and (4) $\text{mcBBR} < 0.6$. More details concerning these steps can be found at the CCS website.⁷

Functional homogeneity

We applied surface-based 2dReHo computation to characterize local functional homogeneity. Specifically, for a given vertex v_0 on the surface grid of interest (*fsaverage5* or *Conte69_32 k*), we identified its K nearest neighbors $v_{1,2,\dots,K}$ and denoted $v_i(t)$ as their RFMRI time series. The 2dReHo measure of this vertex was computed as Kendall’s coefficient of concordance (KCC) among the time series of all nearest neighbors, including itself. The mathematical formula is shown as Eq. (1)

$$\text{KCC} = \frac{\sum_{i=1}^n R_i^2 - n(\bar{R})^2}{\frac{1}{12}K^2(n^3 - n)} = 12 \frac{\sum_{i=1}^n (\bar{R}_i)^2}{(n^3 - n)} - 3 \frac{(n+1)}{(n-1)}, \quad (1)$$

where $R_{i=1,\dots,n}$ represents the ranks of $v_i(t)$, n is the number of time points, \bar{R}_i is the mean rank across its neighbors at

⁷ <http://fcd.psych.ac.cn/QC.html>.

the i th time point, and \bar{R} is the overall mean rank across all neighbors and across all time points. This equation clearly indicates ReHo's advantages in theory, i.e., this metric integrates noise-filtering operations in both the temporal domain (the order-rank filter) and the spatial domain (the mean-rank filter). Thus, this metric has high robustness against temporospatial noise and outliers, which provides this RfMRI metric with high test–retest reliability (Zuo et al. 2013). This computation is repeated for every vertex that has BOLD time series to produce a vertex-wise local functional homogeneity surface map. The ReHo computation is intrinsically a type of spatial and temporal smoothing operation on the cortical surface that is helpful for suppressing the time series noise and for mitigating the inter-individual spatial normalization issue. Length-one (6 neighbors) 2dReHo maps were estimated on the *fsaverage5* surface for the 402 participants from the three sites. Regarding a slightly spatial smoothing (2-mm FWHM) performed for HCP datasets, length-two (19 neighbors) 2dReHo maps were calculated on the *Conte69_32 k* surface for the 80 unrelated HCP participants.

Structural morphology

In this study, the cortical thickness (CT), surface area (SA), mean curvature (CURV), sulcal depth (SD), and local gyrification index (LGI) were estimated to measure different properties of the brain cortical surface morphology. Specifically, the CT was measured in native space millimeters using the averaged linking distance between the pial and white surfaces (Fischl and Dale 2000). This measure of cortical thickness has been demonstrated to show good test–retest reliability across time, scanner manufacturers and field strengths (Han et al. 2006). The SA was set to the total area of the triangles that were connected to a vertex (Fischl and Dale 2000). The total cortical SA yielded by this method shows high agreement with the surface area derived from postmortem studies, has been validated on several brain phantoms, and has been compared with other surface-based analysis packages (Lee et al. 2006; Makris et al. 2006). Given a vertex on the cortical surface, its CURV is the mean of the two principal curvatures, which measure the maximum and minimum bending of the cortical surface at that vertex (Pienaar et al. 2008). The principal curvatures correspond to the maximum and minimum values of normal curvatures, which are generally measured as the inverses of the radii of inscribed circles at the vertex. The SD is the integrated dot product of the movement vector with the surface normal during inflation, which highlights the large-scale geometry of the cortical surface. When deep regions consistently move outward, these regions have positive values of SD, whereas when superficial regions move inward, they have negative values

of SD. The gyrification index is a metric that quantifies the amount of cortex buried within the sulcal folds compared with the amount of cortex on the outer visible cortex. A cortex with extensive folding has a large GI, whereas a cortex with limited folding has a small GI. The computational method of LGI used in the current work computes local gyrification measurements at thousands of points over the entire cortical surface (Schaer et al. 2008).

The metrics described above have potentially distinct geometrical meanings as shape descriptors of the cortical surfaces, motivating their uses in improving the transformation from 3D volume images into 2D surfaces (i.e., performing the surface-based registration) by including more accurate shape information. Additionally, these metrics have been associated with genetic (e.g., Kippenhan et al. 2005; Panizzon et al. 2009; McKay et al. 2013; Vuoksima et al. 2014), neurodevelopmental (e.g., Rettmann et al. 2006; Al-eman-Gomez et al. 2013; Hogstrom et al. 2013; Li et al. 2014; Wright et al. 2014; Lyall et al. 2014), and cognitive/behavioral factors (e.g., Frye et al. 2010; Li et al. 2010; Blackmon et al. 2011; Fjell et al. 2013; Schnack et al. 2014) and with disruptions in various brain disorders (e.g., Levitt et al. 2003; Nordahl et al. 2007; Dierker et al. 2013; Im et al. 2013), underling their anatomical implications. All individual maps of these morphological measures were generated in the native space and then transferred onto the *fsaverage* standard spherical surface. To make these maps comparable with those maps of local functional homogeneity, we also down-sampled all maps of these morphological measures onto the *fsaverage5* standard surface space and spatially smoothed the maps on the surface using a Gaussian filter with a small kernel (FWHM = 4 mm).

Outlier detection procedure

An outlier detection procedure (ODP) was further performed to exclude subjects with extremely low/high measures of both functional homogeneity and structural morphology for ensuring their normal distributions across subjects. For each site, a subject was excluded from the subsequent analyses when any of the six measures observed from this subject was an outlier at any vertex of the *fsaverage5* surface. The outliers were determined using the generalized extreme studentized deviate (ESD) test ($p < 0.001$) (Rosner 1983), which eliminates the masking effect caused by using an underestimated number of possible multiple outliers as the pre-assigned number of these outliers in Grubbs test (Grubbs 1969).

Adjustment for confounding factors

For all subjects passing the QCP and ODP, their maps of both local functional homogeneity and five morphological

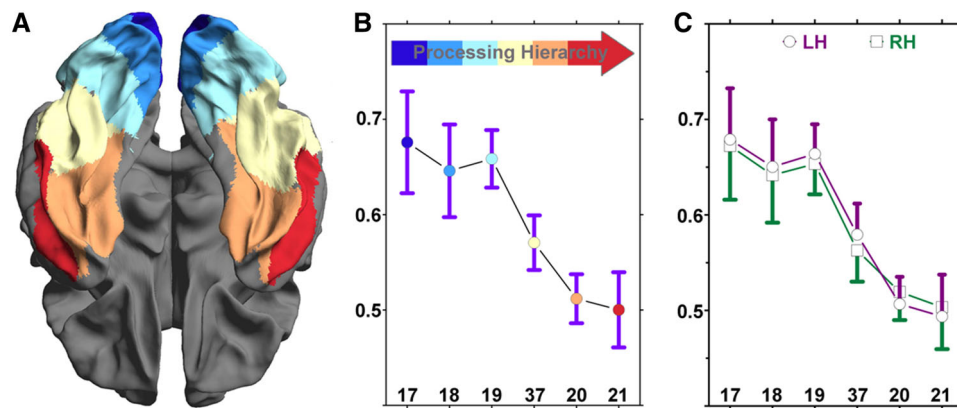


Fig. 2 Regional variation of local functional homogeneity in the ventral visual system. Six areas of Brodmann Atlas (BA) are rendered on the cortical surface (the ventral view of *fsaverage*) (a) and comprise the ventral visual stream and ordered by processing hierarchy (BA17, BA18, BA19, BA37, BA20, and BA21). All

individual mean 2dReHo values are calculated for each of the six areas and plotted across the 402 subjects for both hemispheres (b) or left hemisphere (LH)/right hemisphere, respectively (c). The bar indicates the standard deviation (STD) across the 402 subjects

measures are adjusted for various confounding factors. Specifically, first, a group mask surface is generated to ensure these subjects have nonzero metrics of all vertices in the mask for all six cortical measures. Given a vertex $v \in M$, there are N samples ($Y_i(v), i = 1, \dots, N$) of the cortical measure Y where N is the number of subjects. To account for confounding factors such as site, age, sex, brain size, global mean metric, warp distortion amount and in-scanner motion, linear regression models are employed as shown in Eq. (2):

$$Y_i^{adj}(v) = Y_i(v) - (\beta_{age} \times age_i + \beta_{sex} \times sex_i + \beta_{site} \times site_i + \beta_{gm} \times gm_i + \beta_{icv} \times ICV_i + \beta_{fd} \times meanFD_i + \beta_{bbr} \times mcBBR_i + \beta_{jac}(v) \times JAC_i(v)). \quad (2)$$

In the above equation, to model imaging site variability, subjects from the three sites, Beijing, Cambridge, and Rockland, are represented with numbers 1, 2, 3, respectively. For each of the six metrics Y , its global mean (gm) across the entire cortex is computed by averaging the vertex-wise values of the metric across the entire cortex. The brain size is quantified using the intracranial volume (ICV) estimated using FreeSurfer software. The warp distortion amount for BBR-based function-to-structure realignment is the mcBBR. The in-scanner head motion of frame-wise displacements is measured using the meanFD. To account for heterogeneous changes in regional volume, the amount of regional volume changes required to warp a subject into the standard surface *fsaverage* is measured using the vertex-wise covariate derived from the jacobian determinant of the spherical transform (JAC). Notably, all the above covariates are demeaned (i.e., subtraction of the

mean), and both mcBBR and meanFD are included as covariates for local functional homogeneity adjustment.

Regional variation in local functional homogeneity

To gain structural and neurocognitive insights into the regional differences in local functional homogeneity, we used the adjusted functional homogeneity measure (2dReHo^{adj}) to calculate the mean 2dReHo across vertices within each of the six VVS areas (Fig. 2a), which are labeled with the following Brodmann Atlas (BA) areas: 17, 18, 19, 37, 20, and 21. These areas are ordered by their hierarchies from low to high complexity of information processing (Ungerleider and Haxby 1994) for examining the relation between the changes in 2dReHo and the increased complexity of information across the stream. We employed Friedman tests to examine whether the within-subject rankings of 2dReHo systematically differed across these regions and between subjects.

The hot spots (the highest values) of local functional homogeneity (the upper-left of Fig. 3) were observed within the posteromedial cortex (PMC), and few regional differences were observable within this high-order association area by visual inspection (Zang et al. 2004; Long et al. 2008; Zuo et al. 2013). As shown in the upper-right of Fig. 3, we adopted the PMC masks generated in our previous work (Zuo et al. 2013) by including the four elements of the Destrieux Atlas (Destrieux et al. 2010): (1) the subparietal sulcus (SbPS), (2) the precuneus or medial part of P1 (PrCun), (3) the posterior–dorsal part of the cingulate gyrus (PosDCgG), and (4) the posterior–ventral part of the cingulate gyrus (PosVCgG). With a similar method of analysis for the ventral visual stream, the mean 2dReHo of each subject is calculated for each of the four regions. The

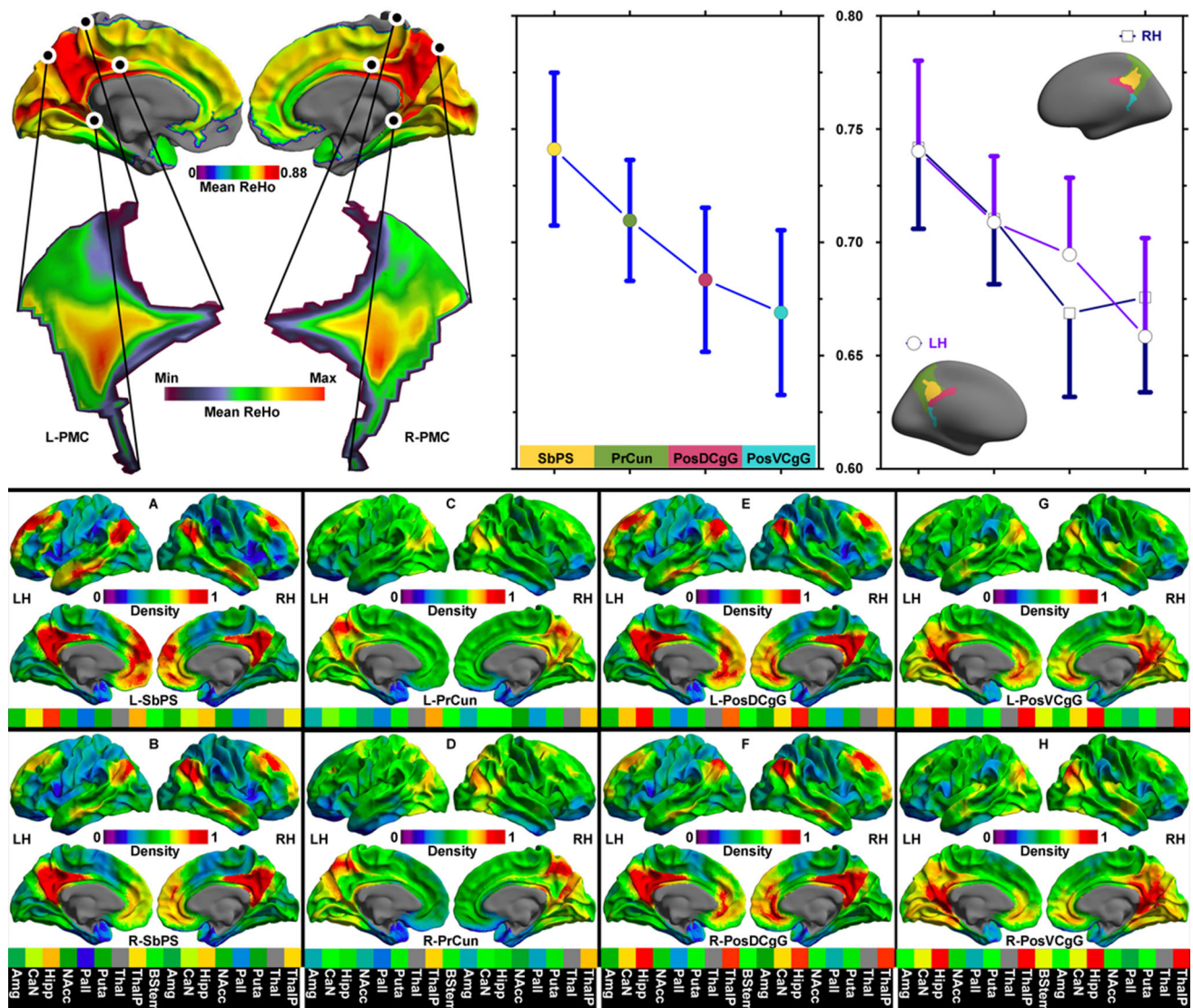


Fig. 3 Local functional homogeneity and connectivity density mapping of the posteromedial cortex. Mean vertex-wise maps of 2dReHo is generated across the 402 subjects and visualized onto the medial surfaces of *fsaverage5*. Regional variations in ReHo within both the left (L-PMC) and right posteromedial cortex (R-PMC) are illustrated via a zoomed-in window of this specific region (*upper-left*). All individual mean 2dReHo values are calculated for each of the four subregions of the PMC (SbPS: subparietal sulcus; PrCun: precuneus; PosDCgG: dorsal part of the posterior cingulate gyrus; PosVCgG: ventral part of the posterior cingulate gyrus) and plotted across the 402 subjects for both hemispheres (*upper-middle*) or left hemisphere

(LH)/right hemisphere, respectively (*upper-right*). The bar indicates the standard deviation (STD) across the 402 subjects. The bottom sub-figures illustrate connectivity density maps of the four PMC subregions for each hemisphere (LH: A/C/E/G; RH: B/D/F/H). All these maps are rendered onto the lateral and medial surfaces of *fsaverage5* and visualized. The mean connectivity density values of 8 subcortical areas (*Amg* Amygdala, *CaN* Caudate, *Hipp* Hippocampus, *NAcc* Nucleus Accumbens, *Pall* Pallidum, *Puta* Putamen, *Thal* Thalamus, *ThalP* Thalamus-Proprius, *BStem* Brain-Stem) are computed and plotted as the color grids at the bottom of each surface rendering

Friedman tests are also used to examine the order of these changes.

To aid our interpretations on the findings of the regional differences in 2dReHo across the four PMC subregions, we proposed a whole-brain connectivity density mapping (CDM) method for each subregion using RfMRI. Specifically, given a subregion P containing N_p vertices, we performed the whole-brain functional connectivity using any vertex $v_n \in P (n = 1, \dots, N_p)$ as a seed based on the

RfMRI time series (Fox et al. 2005). Notably, the RfMRI data used for this analysis were spatially smoothed versions of the preprocessed RfMRI data for 2dReHo computation. The spatial smoothing (FWHM = 6 mm) was first performed for the preprocessed RfMRI time series (see *Image Preprocessing*) on the standard cortical surface *fsaverage* to increase the signal-to-noise ratio and then down-sampled onto the *fsaverage5* surface. The global signal was not removed from the data (Saad et al. 2012). As shown in Eq.

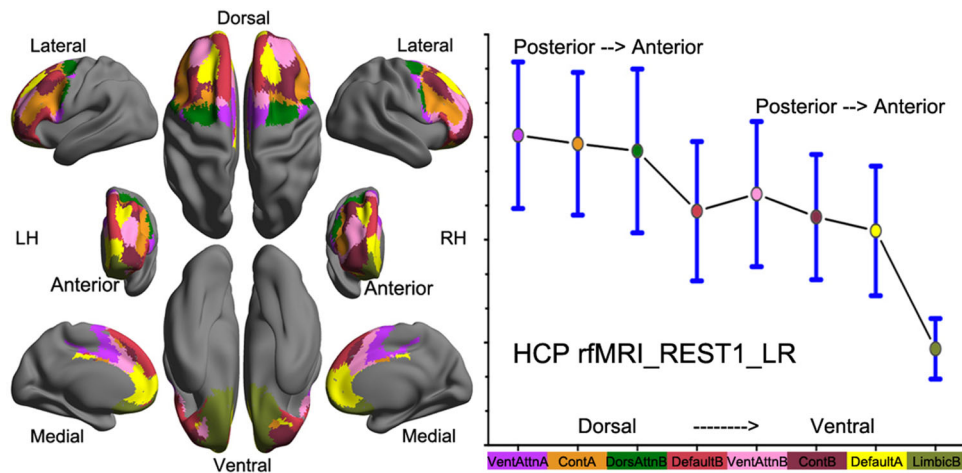


Fig. 4 Functional network hierarchy of local functional homogeneity of the prefrontal cortex. A well-established and highly reproducible functional parcellation is adopted (Yeo et al. 2011) to parcellate the whole brain into 17 functional networks, among which 9 networks covered the PFC: dorsal attention networks A/B (DorsAttnA/DorsAttnB), ventral attention networks A/B (VentAttnA/VentAttnB), control networks A/B (ContA/ContB), default mode networks A/B (DefaultA/DefaultB), and limbic network (Limbic B). Of note, there were only a very small piece of DorsAttnA covered by the PFC, and

we thus merged that piece into DorsAttnB, leading to final 8 PFC networks as illustrated in the *left panel*, namely, VentAttnA, ContA, DorsAttnB, DefaultB, VentAttnB, ContB, DefaultA, LimbicB. This order was ranked along with both dorsal–ventral axis and posterior–anterior axis. The individual mean length-two 2dReHo values across vertices within each of the 8 PFC networks for each of the four RFMRI scans of all 80 HCP participants are computed and plotted in the *right panel*

(3), given a vertex $v_m \in M$ ($m = 1, \dots, N_M$) where M is the group surface mask, its connectivity density to the region P is defined as the proportion of vertices within P showing significant functional connectivity, as measured using a temporal correlation of the time series (ts) to the vertex v_m .

$$\rho(v_m) = \frac{\#\{v_n \in P | \text{corr}(ts(v_n), ts(v_m)) > = 0.2\}}{N_p} \quad (3)$$

To examine the connectivity density of subcortical regions, the mean time series were extracted by averaging the time series of all voxels within each of 17 subcortical regions based on the preprocessed RFMRI data in individual native volumetric spaces. The masks of these subcortical regions were first generated in individual native anatomical spaces using the segmentation procedure in FreeSurfer software and then transformed to the corresponding individual functional spaces using the BBR-based co-registration, namely, Amygdala (Amg), Caudate (CaN), Hippocampus (Hipp), Nucleus Accumbens (NAcc), Pallidum (Pall), Putamen (Put), Thalamus (Thal), Thalamus-Proper (ThalP) for each hemisphere, and Brain-Stem (BStem). The connectivity densities of the 17 regions were calculated using the same method as those densities of cortical regions in Eq. (3). The choosing of a high correlation threshold for significant functional connectivity was inspired by a previous study (Buckner et al. 2009). Selections of different thresholds did not qualitatively change our findings. Only the NKI/Rockland lifespan datasets were used for this analysis.

The functional organization of the PFC remains poorly understood. To understand the functional hierarchy of the network organization in the PFC, we adopted a well-established and highly reproducible functional parcellation recently developed by Yeo et al. (2011) based on RFMRI datasets from 1000 healthy participants. The entire brain was parcellated into 17 functional networks, among which the following 9 networks overlapped with the PFC: dorsal attention networks A/B (DorsAttnA/DorsAttnB), ventral attention networks A/B (VentAttnA/VentAttnB), control networks A/B (ContA/ContB), default mode networks A/B (DefaultA/DefaultB), and the limbic network (Limbic B). Notably, there was only an extremely small piece of DorsAttnA covered by the PFC; thus, we merged that piece into DorsAttnB, leading to 8 final PFC subnetworks, as illustrated in the left panel in Fig. 4, namely, VentAttnA (overlapping with BAs 6, 24 and 4), ContA (overlapping with BAs 44, 6 and 46), DorsAttnB (overlapping with BAs 6 and 4), DefaultB (overlapping with BAs 6 and 4), VentAttnB (overlapping with BAs 8, 9, 46, 11, 6, 45 and 47), ContB (overlapping with BAs 10, 11, 8, 9 and 6), DefaultA (overlapping with BAs 8, 10, 32, 24, and 9), and LimbicB (overlapping with BAs 11 and 25). This order was ranked along with both the dorsal–ventral axis and the posterior–anterior axis. Using a similar method, we derived the individual mean length-two 2dReHo values across vertices within each of the 8 PFC networks for each of the four RFMRI scans of all 80 HCP participants. Friedman tests were utilized to examine whether the within-participant

rankings systematically differed across these regions and between participants.

Morphological association with local functional homogeneity

A vertex-wise multiple linear regression was employed to estimate the linearly structural contribution to 2dReHo, as formulated in Eq. (4),

$$2dReHo_i^{adj} = \mu + \beta_{CT} \times CT_i^{adj} + \beta_{SA} \times SA_i^{adj} + \beta_{CURV} \times CURV_i^{adj} + \beta_{SD} \times SD_i^{adj} + \beta_{LGI} \times LGI_i^{adj} + e_i. \quad (4)$$

For each vertex on the *fsaverage5* surface, the percentage of variances of the adjusted 2dReHo that was explained by each of the five structural metrics was estimated by solving the regression model (4). The partial correlation coefficients between the adjusted 2dReHo and each of these morphological measures and their statistical significances were also computed from the multiple linear regression (4). Then, the final *p* value maps of these significant associations were corrected for multiple comparisons using FDR ($p < 0.05$).

For delineating the covariation of spatial distribution patterns between the functional homogeneity and morphology, first, we computed the mean maps of 2dReHo and the five morphological metrics across all subjects passing both QCP and ODP from the three imaging sites. Then, the Kendall's rank correlation coefficients of the spatial maps between 2dReHo and each of the five structural metrics (the CT, SA, CURV, SD, and LGI) were estimated and further visualized as the two-dimensional histograms by enhancing scatterplots with smoothed densities (Eilers and Goeman 2004).

Functional covariance network of local functional homogeneity

To investigate the inter-regional covariation pattern of local functional homogeneity across subjects within the entire cortical mantle, a whole-brain vertex-wise covariance network of 2dReHo^{adj} (i.e., a covariance connectome) was generated. Due to the intrinsic feature of spatial smoothing in the ReHo computation, we decided to down-sample the 2dReHo^{adj} from the *fsaverage5* surface to the *fsaverage4* surface (2,562 vertices per hemisphere, with a 5.5-mm neighboring-vertex distance), eliminating all possible artificially introduced connections between any pair of geometrically neighboring vertices in the *fsaverage5* grid. For any pair of vertices (*u*, *v*) on the *fsaverage4* surface, their inter-vertex covariation was determined using the

inter-vertex correlation across subjects $corr(2dReHo^{adj}(u), 2dReHo^{adj}(v))$. A *p* value of 0.001 was used to threshold these correlations (Zuo et al. 2012), resulting in an adjacency matrix, which is a binary graphical description of the complete set of brain connections, i.e., a brain connectome (Sporns et al. 2005). Both the degree centrality (DC) and betweenness centrality (BC) were computed to characterize the network connectivity pattern (Rubinov and Sporns 2010) and the putative hubs within these connectomes of functional homogeneity covariance using multiple network centrality metrics (Zuo et al. 2012).

Then, the degree distribution of the 2dReHo-derived connectome was modeled using an exponentially truncated power-law function regarding previous voxel-wise brain network analyses (Hayasaka and Laurienti 2010) and compared with exponential and power-law models (He et al. 2009). To further examine the hierarchy and modular organization of the 2dReHo-derived connectome, we applied a fast algorithm of unfolding communities in large networks (Blondel et al. 2008) to the functional covariance network. More details concerning this algorithm can be found in the previous study (Zuo et al. 2012). The visualization procedure was completed using a Mac Pro graphics workstation armed with 24 CPU cores, 64 GB RAM, and an ATI Radeon HD5770 video card (1 GB physical memory).

Results

Overall, 132 subjects from the Beijing sample, 159 subjects from the Cambridge sample and 111 subjects from NKI/Rockland sample passed our QCP and ODP, as detailed in the “Materials and Methods” section, resulting in 402 usable datasets across the three sites. Basic information describing these participants is shown in Table 2, including age range, gender, ICV, mcBBR and meanFD.

Regional variation in local functional homogeneity

In the present study, the local functional homogeneity of the human brain architecture across a large sample was mapped vertex-wise onto the cortical mantle for the first time. The vertex-wise high-resolution 2dReHo maps allowed us to examine the spatial distribution details for insights into regional variations. This measure exhibited rich regional variations across the cortical mantle, whereas its overall spatial pattern was highly similar to the previous observations in a small sample (Zuo et al. 2013).

The Friedman test concerning the presence of region ordering within the ventral visual stream (the purple curve in Fig. 2b) revealed robust changes in 2dReHo ($p < 1e-$

Table 2 Basic information for participants with usable datasets

	Beijing (<i>N</i> = 132)	Cambridge (<i>N</i> = 159)	Rockland (<i>N</i> = 111)	Combined (<i>N</i> = 402)
Age (Years)	21.3 ± 2.05	21.0 ± 2.24	37.1 ± 20.80	25.5 ± 13.15
Age range (Years)	18.0–28.0	18.0–30.0	8.0–85.0	8.0–85.0
Gender (Males)	47	55	61	163
ICV ^a (Liter)	1.1 ± 0.14	1.2 ± 0.17	1.2 ± 0.20	1.2 ± 0.17
mcBBR ^b	0.5 ± 0.04	0.4 ± 0.05	0.5 ± 0.05	0.5 ± 0.06
meanFD ^c (mm)	0.04 ± 0.023	0.04 ± 0.021	0.08 ± 0.039	0.05 ± 0.0317

^a ICV is the intracranial volume

^b mcBBR is the minimal cost of the intra-subject co-registration with the boundary-based registration

^c meanFD is the mean frame-wise displacement for in-scanner head motion

10): BA17 (0.564), BA18 (0.531), BA19 (0.533), BA37 (0.424), BA20 (0.345) and in BA21 (0.344). This order of regional changes in 2dReHo is reproducible across the two hemispheres (Fig. 2c). Within the PMC, the ReHo exhibited both anterior–posterior and dorsal–ventral gradients (upper-left of Fig. 3), where a robust ordering pattern of regional differences in 2dReHo across the four subregions of the PMC ($p < 1e-10$) was confirmed by the Friedman test (upper-middle of Fig. 3): the SbPS (0.741), PrCun (0.710), PosDCgG (0.683) and PosVCgG (0.670). This ordering of 2dReHo regional variations is robust across the two hemispheres, except for the PosVCgG (upper-right of Fig. 3).

The CDM analysis revealed that (1) SbPS highly connects to the medial prefrontal cortex (MPFC), lateral parietal cortex (LPC), dorsal lateral prefrontal cortex (DLPFC) and to the anterior temporal cortex (Fig. 3a, b); (2) PrCun has the highest density of functional connectivity with the visual cortex and with the DLPFC (Fig. 3c, d); (3) the PosDCgG demonstrates the most dense functional connectivity with the anterior and ventral parts of the MPFC (i.e., the aMPFC and vMPFC), LPC, DLPFC, temporal cortex and two subcortical regions (the Hipp and ThalP) (Fig. 3e, f); (4) the PosVCgG mutually connects to the medial visual cortex, vMPFC, Hipp, ThalP, LPC, DLPFC and to the posterior insular cortex with the highest connectivity density (Fig. 3g, h).

The PFC shaped its 8 functional networks into a hierarchical organization of the local functional homogeneity with the following order, which is shown in Fig. 4: VentAttnA, ContA, DorsAttnB, DefaultB, VentAttnB, ContB, DefaultA, and LimbicB. This hierarchical structure was statistically robust within and between subjects and confirmed by the Friedman test (all p values $< 1e-10$). The within-network gradient of 2dReHo is evident along the dorsal–ventral axis for the three major networks, ventral attention, control and default networks. The between-network gradient of 2dReHo essentially matches the posterior–anterior axis.

Morphological association of local functional homogeneity

Figure 5 summarizes the main findings concerning the morphological association of 2dReHo. The first column of Fig. 5 demonstrates the mean surface maps of the five common morphological measures. The two-dimensional histograms of the mean 2dReHo map and each mean morphology map are visualized, as shown in the third column. Our rank-based spatial correlation analyses revealed significant relations (all p values $< 1e-25$) of spatial patterns between 2dReHo and the following morphological measures: (1) CT: Kendall tau = -0.1074 ; (2) SA: Kendall tau = -0.1556 ; (3) CURV: Kendall tau = 0.3897 ; (4) SD: Kendall tau = 0.2496 ; (5) LGI: Kendall tau = 0.1900 . The second column depicts the cortical surface mapping of the vertex-wise partial correlation between 2dReHo and each of the five structural metrics. Widely distributed negative correlations between the surface area and 2dReHo were detected regionally across the cortex where the posterior–dorsal part of the cingulate gyrus exhibited the highest area-homogeneity association (the second row). The functional homogeneity of the parieto-occipital sulcus, marginalis cingulate sulcus and of the cingulate cortex exhibited significant positive correlations with the CT (the first row). The CURV exhibited high positive correlations with 2dReHo in a variety of sulcal clusters distributed in the frontal, temporal, parietal and in the occipital cortex, particularly the positive correlations along the cingulate sulcus (the third row). 2dReHo showed significant negative correlations with the SD in several temporal and parietal clusters and with the aMPFC (the fourth row). Significant positive correlations between LGI and 2dReHo were observed in the DLPFC and in the middle temporal gyrus (the fifth row). Over 88 % of the variances in local functional homogeneity across subjects were unique to each of the five morphology measures, which only account for or explain less than 12 % of the variability of 2dReHo.

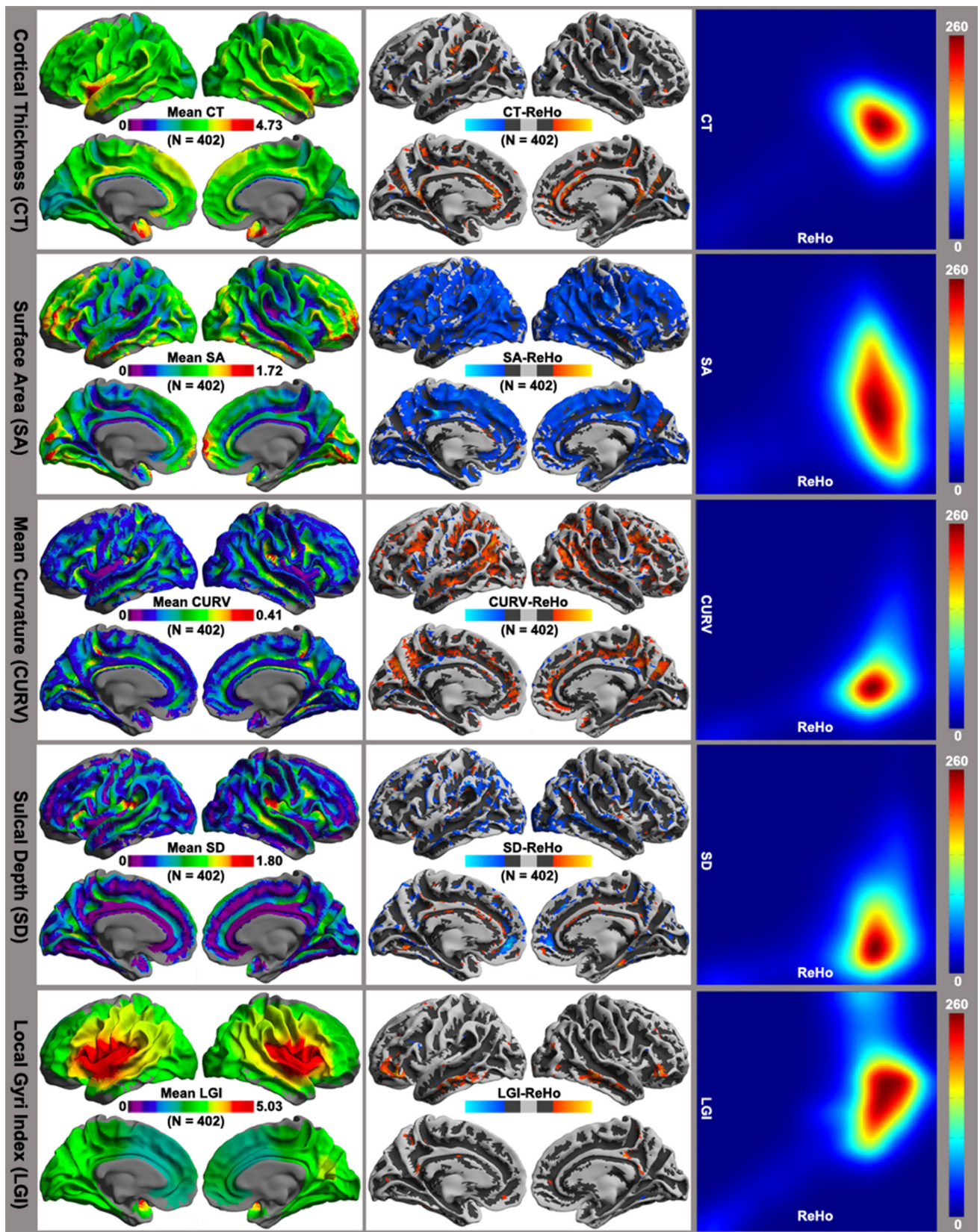


Fig. 5 Morphological association of local functional homogeneity. The mean maps of the five measures of structural morphology (*CT* cortical thickness, *SA* surface area, *CURV* mean curvature, *SD* sulcal depth, *LGI* local gyrification index) are calculated across the 402 subjects and rendered onto the *fsaverage5* surfaces (the *first column*). The two-dimensional histograms of the mean map of 2dReHo and mean maps of each of the five morphological measures are displayed as in the *third column*. The significant partial correlations between 2dReHo and each of the five morphological measures are displayed on the *fsaverage5* surfaces (the *second column*)

Functional covariance network of local functional homogeneity

The community detection algorithm produced five modules (bottom-right in Fig. 6) by maximizing the modularity $Q_{\max} = 0.62$ of the functional covariance network derived by local functional homogeneity (2dReHo). The largest (41.72 % nodes) module (I) includes high-order association areas, such as the frontal, parietal and temporal cortices, representing an association network. The second (20.89 % nodes) module (II) is a motor network containing both the pre- and post-central cortex as well as the posterior portion of the insular cortex. The third (15.65 % nodes) module (III) primarily covers the occipital cortex, namely, a visual network. In the remaining two modules, one module (IV) is in the primary temporal cortex as an auditory network (9.75 % nodes), whereas another module (V) appears to contain nodes of boundaries between the high-level module (I) and the other three low-level modules (II, III, and IV), leading to a transition network (11.99 % nodes). The adjacency matrix of the functional homogeneity connectome is depicted in Fig. 6, representing a high-resolution vertex-wise covariance connectome with 4,389 nodes and with 752,404 edges. Notably, this brain graph is fully connected and has a connection density of 3.9 %. The order of vertices in this adjacency matrix was followed that of the five modules. The adjacency matrix of the 2dReHo-derived connectome was further rendered onto the cortical surface, showing only the inter-module edges (bottom-left in Fig. 6).

Compared with pure power-law distribution and with a pure exponential distribution, both the degree centrality (DC) and betweenness centrality (BC) of this connectome appear to demonstrate an exponentially truncated power-law distribution across nodes (DC: Fig. 7b; BC: Fig. 7d) although this distribution explains the much lower variability of the empirical BC data compared with the DC data (46.4 vs. 78.5 %). This distribution indicates that this functional covariance network is not a scale-free network, implying a lower probability of nodes with extremely high centrality metrics due to physical constraints or associated with a cost (Amaral et al. 2000). Figure 7a and c show the network centrality maps of the functional covariance

network, revealing a set of hub regions, including the visual, the post-central cortex, the supplementary motor area, the posterior insula, the DLPFC and the aMPFC. Although both the DC and BC indicate the same set of network hub regions, the BC tends to emphasize the high-order areas (the posterior insula, DLPFC and aMPFC); however, the DC more emphasizes the primary sensory areas (the visual, the post-central cortex, and the supplementary motor area). This result is not surprising considering that the BC characterizes a more global feature of the information flow in the network, whereas the DC is a local characterization of this information.

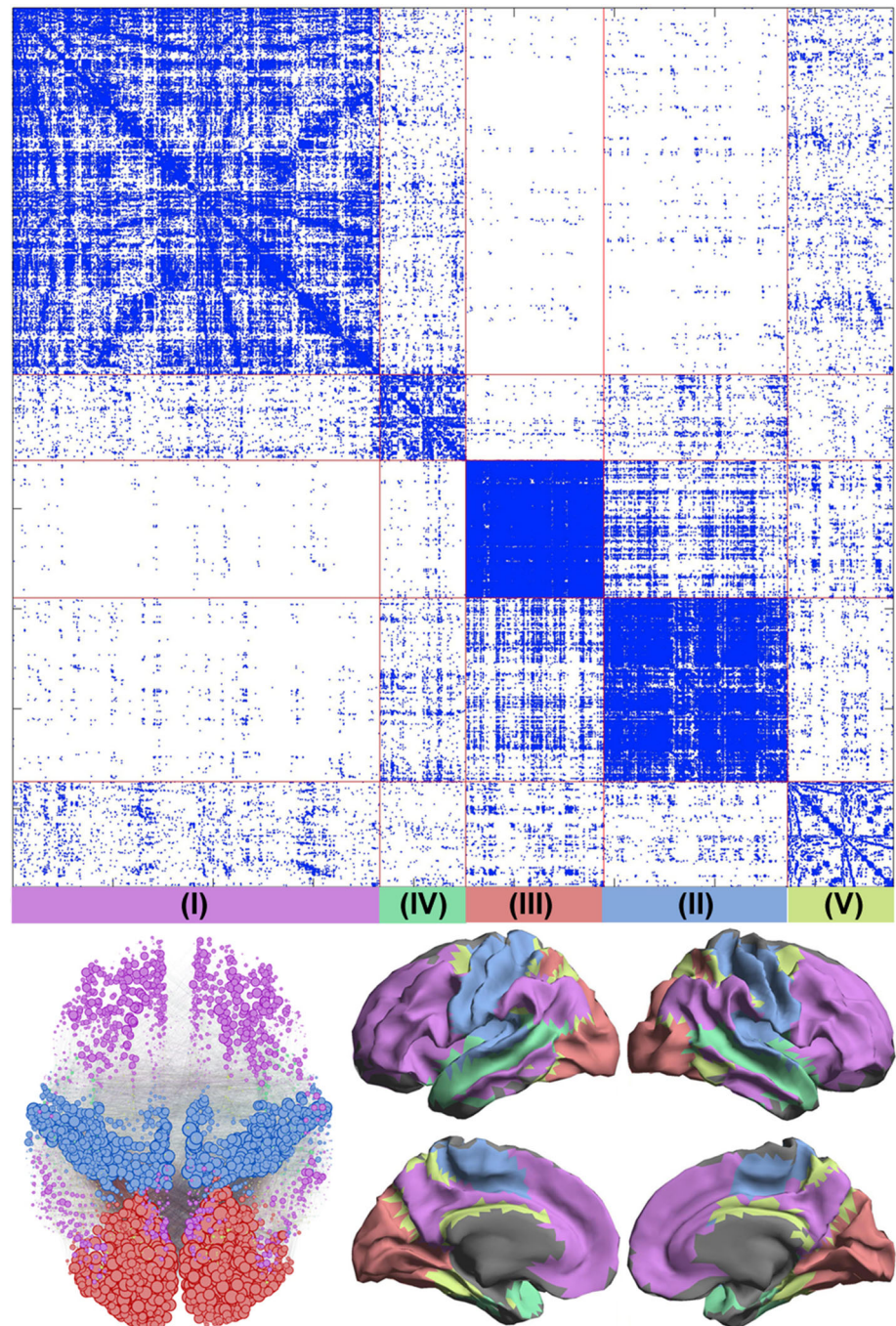
Reproducibility and reliability

This study combines 402 samples from three different imaging sites to increase the statistical power in the proposed analyses. RFMRI-based functional connectomics has been demonstrated to be sensitive to various factors including the imaging sequences (Yan et al. 2013b). Therefore, it is crucial to examine the reproducibility of our findings across three imaging sites. Accordingly, we repeated all the analyses proposed in the “Methods” section for each individual imaging site. The results of the reproducibility analysis confirmed that all the findings reported above were reproducible across the three sites. Due to space limitations, we only presented the reproducibility of the results of regional variation in this study. The matching of local functional homogeneity and the hierarchy of information processing in the ventral visual stream were highly reproducible across the three sites (the first row in Fig. 8). Similarly, the gradient of local functional homogeneity within the four subregions of the PMC was highly reproducible and robust across the three sites (the second row in Fig. 8). Finally, the functional hierarchy of the PFC was highly test–retest reliable across the four RFMRI scans within 2 days, exhibiting almost identical network orders (the third row in Fig. 8).

Discussion

Local functional homogeneity varies markedly across the human cortical mantle and its functional covariance across individuals indicates a whole-brain network with a hierarchically organized modular structure. A posterior–anterior decreasing gradient is obvious for the overall pattern of the spatial distribution of local functional homogeneity. The increases in local functional homogeneity reflect a reduced complexity of information processing or hierarchies of functional segregation and integration within the ventral visual stream. Consistently, gradients of local functional homogeneity along the subregions of a multimodal high-

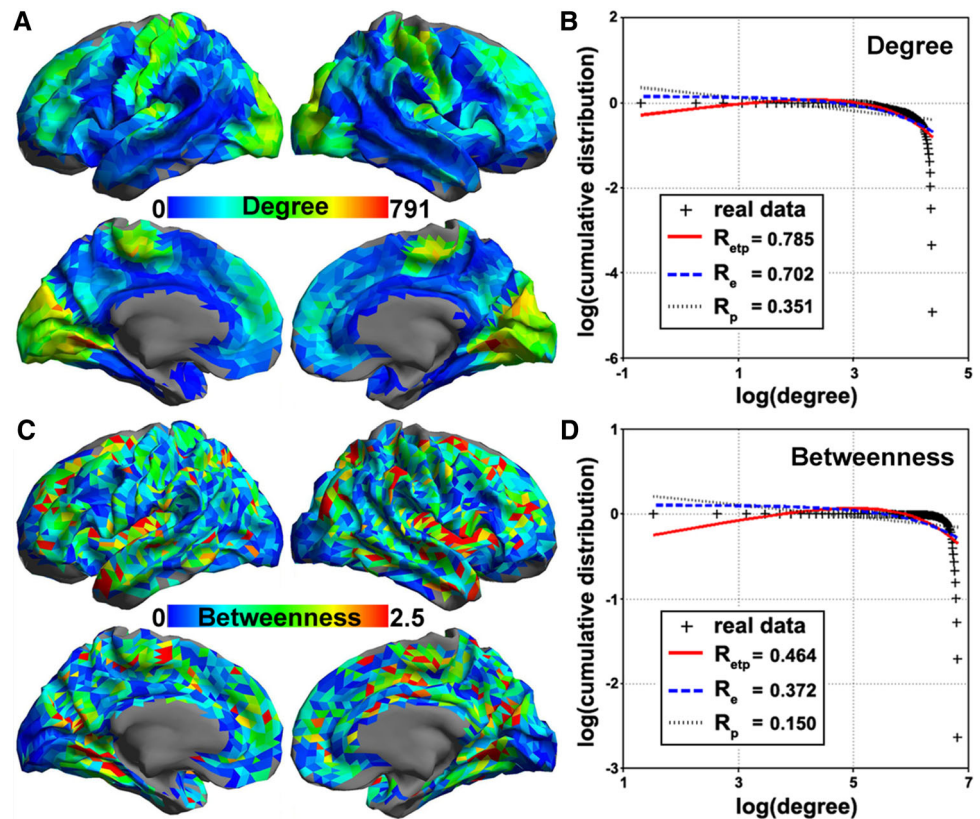
Fig. 6 Functional covariance network and its modules. The adjacency matrix of whole-brain vertex-wise functional covariance network derived with the inter-regional covariation of 2dReHo is depicted as the up of the plot, representing a fully connected brain graph with 4,389 nodes and 752,404 edges (connection density: 3.9 %). There are five modules (I: association module; II: sensory motor module; III: visual module; IV: auditory module; V: transition module) detected by the community detection algorithm applied to this matrix and rendered onto the fsaverage4 surfaces (*right-bottom*). The order of vertices in this adjacency matrix is according to the five modules as the *red lines* outline. The adjacency matrix the connectome is further rendered onto the cortical surface with showing only the inter-module edges (*left-bottom*) by using Gephi (<https://gephi.org>)



order association area, the posteromedial cortex (PMC), mirror the degree of the multimodal integration in processing information reflected in the functional anatomy of the PMC. A functional hierarchy of sub-networks is detectable for the human PFC, echoing its network-level organization of ventral attention-cognitive control-default networks. The whole-brain inter-regional covariation of local functional homogeneity across individuals is organized into a complex network with five biologically meaningful and hierarchically organized large-scale

modules. Network centrality analyses of this functional covariance network detect hubs of both primary sensory and high-order association areas. Finally, the functional homogeneity exhibits significant correlations with the cortical morphology, thus revealing the potential structural basis of the local functional activity. In the following sections, we explore the details of these maps and discuss what the above findings suggest concerning the neurobiological importance of local functional homogeneity and the significance for functional connectomics.

Fig. 7 Functional covariance network centrality mapping. Network centrality maps are rendered on the fsaverage5 surfaces for (a) degree centrality and (c) betweenness centrality. Log–log plots of the cumulative probability of nodal centrality distribution are also plotted for (b) degree centrality and (d) betweenness centrality. The red solid, blue dashed and black dotted lines indicate the fits of exponentially truncated power law [$p(x) \sim x^{-\alpha-1} e^{-\lambda/x^c}$], exponential [$p(x) \sim e^{-\lambda/x^c}$], and power law [$p(x) \sim x^{-\alpha-1}$], respectively. R-squared values indicate the goodness of the fits (R_{etp} R-squared value for an exponentially truncated power-law fit, R_e R-squared value for an exponential fit, R_p R-squared value for a power-law fit)



Biological meanings of local functional homogeneity

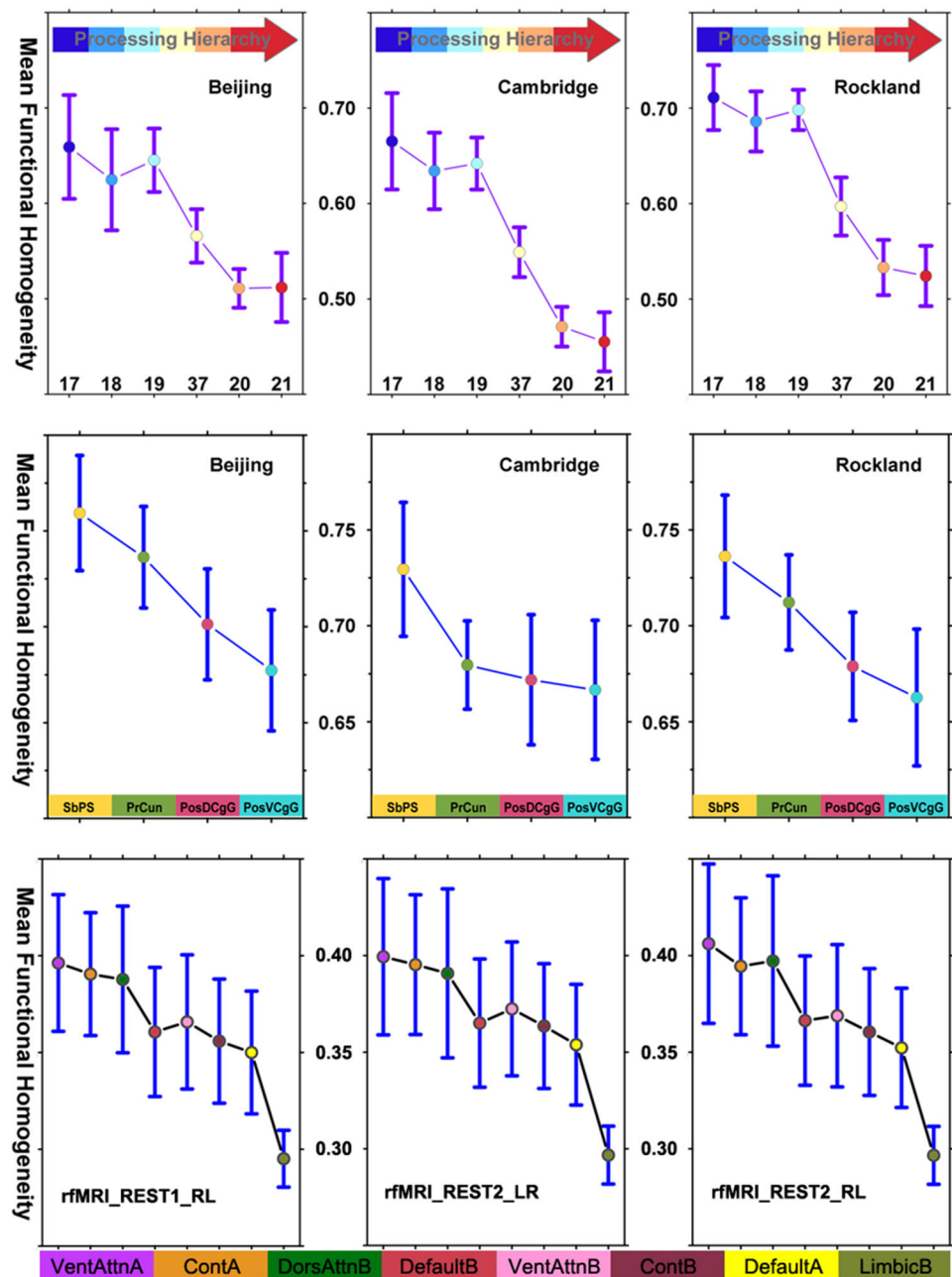
Mapping functional homogeneity illustrates the gradient distribution of the functional homogeneity across the cortical mantle and suggests that this measure most likely reflects the degree of regional segregation in human brain function. ReHo is an index of local functional connectivity or synchronization (Zang et al. 2004; Zuo et al. 2013) and has been related to functional segregation as a short-distance connection (Sepulcre et al. 2010). As strong support for this speculation regarding the functional meaning of regional homogeneity, the information processing hierarchy in the ventral visual stream is perfectly matched with its regional gradient order of functional homogeneity, thus adding an indication of the complexity of information processing into the neurocognitive meanings of regional segregation.

The examination of the local functional anatomy of the PMC and of the PFC also provides similar evidence. Quantitative tests showed a highly reproducible and statistically robust order of 2dReHo along the four subregions of the PMC. The sub-parietal sulcus primarily connects to high-order association areas (Fig. 3a, b) and thus exhibits the highest functional homogeneity. Beyond the high-order connectivity, the precuneus extends its connectivity to visual areas (Fig. 3c, d) and leads to lower functional

homogeneity than the sub-parietal sulcus. By adding sub-cortical connectivity (primarily with the hippocampus and with the thalamus), the dorsal PCC and ventral PCC are more functionally heterogenous with the ventral PCC as the most functionally heterogenous or with the lowest functional homogeneity regarding its connectivity with multiple primary sensory areas and with the insula. Our findings suggest that the functional homogeneity reflects the degree of multimodal information integration within the PMC. These findings provide new insight into the clear boundaries in the PMC regarding its anterior–posterior and dorsal–ventral changes in functional homogeneity and in its functional anatomy (Margulies et al. 2009; Cauda et al. 2010; Zhang et al. 2014).

Similarly, at network level, the PFC encodes the dorsal–ventral and posterior–anterior gradients of local functional homogeneity into its network topology. Part of the limbic network (i.e., LimbicB or the orbital frontal cortex) exhibits the lowest homogeneity. This finding could indicate the actual reflection of the functional heterogeneity within this region or of the low quality of BOLD signal detection in this region. Notably, the HCP Q3 data were used for this analysis, and thus, we expected low homogeneity as an indication of function. Beyond this network, our findings revealed a novel gradient of functional homogeneity across the following three high-order

Fig. 8 Reproducibility of regional variation in local functional homogeneity. This figure illustrates the reproducibility of regional variation in local functional homogeneity for ventral visual stream (*top panel*) and the posteromedial cortex (*middle panel*) across the three imaging sites (Beijing, Cambridge and Rockland). The *bottom panel* demonstrates the reproducibility of the network-level functional homogeneity variation for the prefrontal cortex across the three multiband RFMRI sessions (rfMRI_REST1_RL, rfMRI_REST2_LR, rfMRI_REST2_RL). The legends of the X-axis are consistent with those legends of Figs. 2, 3, 4



association networks: attention, cognitive control and default networks. The main function of the PFC has been assigned to human cognition, which has been increasingly characterized as an emergent property of interactions among distributed, functionally specialized brain networks (McIntosh 2000). Interestingly, although limited in the PFC, the attention network is primarily driven by external stimulation (the highest functional homogeneity), whereas the default network is related to internal self-related experiences (the lowest functional homogeneity). Recent studies have demonstrated a complex, distributed and

dynamic interaction among the three networks (Luckmann et al. 2014; Elton and Gao 2014; Andrews-Hanna et al. 2014). These recent advances concerning inter-network connectivity increasingly support a role of the control network as a feasible modulator between the other two networks, i.e., the modulation between external goal-directed stimulation and internal self-generated thought (Spreng et al. 2013; Cole et al. 2013; Zanto and Gazzaley 2013). The level of local functional homogeneity in the control network between the other two networks might reflect this network organization of the human PFC. The

full picture of the functional hierarchy in the PFC revealed by 2dReHo represents a novel addition to the current knowledge concerning the human PFC by linking the functional hierarchy findings, which were delineated based on sophisticated cognitive task fMRI (e.g., Badre and D'Esposito 2007, 2009; Badre 2008), to hierarchical functional network organization revealed by RFMRI. This finding has important consequences on the interpretation of previous task-based local functional homogeneity studies (e.g., Tian et al. 2012; Wang et al. 2014).

The module organization that was revealed by the functional covariance network (FCN) derived using 2dReHo added novel insight into the human brain architecture. The distinction between the association module and the primary sensory module has rarely been demonstrated using resting-state functional connectivity approaches. One exception can be found in Zhang et al. (2011), in which the FCNs based on the amplitude of low-frequency fluctuations revealed a similar distinction. However, in many ways, this network organization is different from those network organizations in recent resting-state functional connectivity studies (Yeo et al. 2011; Power et al. 2011; Zuo et al. 2012; Wig et al. 2013). For example, the fronto-parietal cortices are organized into several distinct networks in those previous studies; however, these cortices appear integrated into a large association module. The default mode network is also another cardinal network that seems to be less prominent in the current study, which is also part of the same association module. This finding suggests that the covariance of 2dReHo might be pretty different from conventional resting-state correlations. This covariance pattern seems closer to anatomical organization but does not directly reflect the functional coupling of segregated brain systems.

The FCN analysis indicates a possible role of neurodevelopmental factors in organizing functional homogeneity into a brain connectome. The structural covariance in the human cortex has increasingly been recognized to reflect developmental coordination or synchronized maturation between brain areas (Mechelli et al. 2005; He et al. 2007b; Alexander-Bloch and Giedd 2013). In this study, we demonstrated for the first time the topological organization and modular structure of the high-resolution covariance network of functional homogeneity in the human brain. The functional covariance network is organized with a clear hierarchy of the five modules: three primary sensory (visual, motor and auditory) modules developed early and one high-order association (fronto-parieto-temporo) module developed late, as well as one transition module on the boundaries between primary sensory and association modules. This topology may be an indication of inter-regional relations in processing information or in developing cognitive capacities during brain development. The

network centrality metrics (both degree and betweenness) follow an exponential truncated power-law distribution, implying a physically embedded complex network with a limitation on its wiring cost (Bullmore and Sporns 2009). Highly connected nodes (i.e., hubs) within the network architecture are clearly categorized into primary sensory areas (the visual and sensory motor cortices) and high-order association areas (the DLPFC, aMPFC and insula). These sensory motor areas (particularly bilateral precentral cortex) have been demonstrated to play the role of the “rich club” within the connectomes to form its central communication backbone (van den Heuvel and Sporns 2011; van den Heuvel et al. 2012; Collin et al. 2013). Interestingly, the degree centrality map of the functional homogeneity covariance network (Fig. 6a) exhibits a highly similar spatial pattern to those patterns of myelin maps (Fig. 3 in Glasser and Van Essen 2011). This finding indicates a potential link in neurodevelopment between structure and function regarding the inter-regional covariation in functional homogeneity.

In further consideration of the neurodevelopment link in complex network theory, the combined feature of highly connected nodes (hubs) and of hierarchical modules has been proposed as a principle of both segregated and integrated information processing (Tononi et al. 1994; Sporns et al. 2000; Tononi and Sporns 2003; Basset and Bullmore 2006; Gallos et al. 2012). Considering this view with the background of brain development, segregated (or specialized) information processes related to primary sensory functions, would benefit from highly connected topological neighbors and could be developed first. In contrast, integrated (or distributed) information processes related to high-order cognition such as executive functions, would benefit from global information transfer following the hierarchy of modular organization, which produces the delay in the development of these functions to the primary sensory functions. Our findings are consistent with the previous developmental studies (Gogtay et al. 2004). The detection of these patterns of functional covariance reveals five functionally well-segregated and hierarchically integrated modules, suggesting that such a functional covariance network encodes the neurodevelopmental aspects of the human cognitive capacities (Zhang et al. 2011; Alexander-Bloch et al. 2013).

Functional homogeneity and brain connectomics

Our results provide additional insight into human brain connectomics. Brain connectomics is facing various challenges, as discussed by Sporns (2013). The first challenge concerns the mechanism underlying the structure–function relation. Using 2dReHo, we demonstrated this linear relation between functional homogeneity and

cortical morphology. However, the linear structure–function relation appears to be capable of interpreting a small portion (<12 %) of the variability. This observation should motivate studies concerning this relation using biologically plausible physical models of the human brain (normally nonlinear) (Cabral et al. 2011; Deco and Jirsa 2012; Nakagawa et al. 2013, see Deco et al. 2013 for review). The second challenge is to create a meaningful definition of the nodes in the connectome. Beyond the multiple-scale nature of both structure and function in the human brain, our findings showed a striking gradient of the regional variations in local functional homogeneity, particularly calling into question how a brain graph node can be reasonably determined with appropriate considerations of the regional functional homogeneity changes. This finding somehow challenges the predefined brain parcellation strategies and demands a more sophisticated brain parcellation that considers regional variation and individual variability in both the structure and function of the human brain at the group and individual levels. From a functional perspective, regional homogeneity offers a suitable starting point for parcellating the brain into elements of its function at both group and individual levels (e.g., Blumensath et al. 2013). For large-scale brain connectome analysis (50–200 nodes), the connectivity density mapping we proposed in this work could provide a satisfactory choice for defining more reasonable edges regarding the regional variation of local functional homogeneity.

The final challenge is how to account for the individual differences when building a connectome, particularly a functional connectome. Both inter- and intra-individual differences in the brain structure and function have been demonstrated to have biologically meaningful parts (MacDonald et al. 2006; Van Horn et al. 2008; Kanai and Rees 2011; Garrett et al. 2013), both of which contribute to the test–retest reliability of structural and functional measures. In our previous work, functional homogeneity was demonstrated to be a highly test–retest reliable functional measure (Zuo et al. 2013). In this study, we demonstrated that individual differences can be helpful for mapping the regional variation, inter-regional covariation and morphological association of local functional homogeneity and can lead to a novel approach for building a vertex-wise functional covariance network.

Limitations and directions

Several limitations should be considered in interpreting the current findings. First, the subcortical areas were excluded from our present analysis because these areas were not of interest at this time. No aspects of functional homogeneity presented in this study should be generalized to these

regions until directly examined in future work. Second, the linear correlation may be too simple to examine the structural basis of functional homogeneity, particularly when we consider the entire brain cortex. In the future, a computational modeling study could be employed to directly examine these associations within a small region of the human brain and provide insights into the structure–function relation. Third, fMRI data usually contain various physiological noises and are sensitive to various confounding factors (Yan et al. 2013b). The individual differences in functional homogeneity not only reflect the inter-individual variability of the local connectivity but also may indicate the variability of vascular structures across individuals. However, the high test–retest reliability of the 2dReHo metric (Zuo et al. 2013) and the reproducibility of the current findings mitigate this concern. Specifically, 2dReHo is an adaptive noise-suppression approach to quantify local functional homogeneity. We controlled for various nuisance signals, including those signals associated with vascular factors, and obtained highly reproducible findings across the three imaging sites. Fourth, in concluding the developmental implications of this covariance network analysis, notably, these conclusions were speculative in nature because we were not directly evaluating the age effects on 2dReHo but rather based the discussion on previous structural covariance network studies. 2dReHo-derived structural covariance matrices were constructed across subjects encompassing a rather large lifespan age range, and thus, we concluded that any coherent pattern should reflect synchronization across the lifespan. How to evaluate the age effects and how to construct a statistical model (e.g., a linear or quadratic term) for structural covariance networks remain open questions because all individual features (e.g., age) were wrapped into the covariance networks at the group level. One possible method of examining the age effects on the covariance network is to have sufficient samples across every age spans, to construct the covariance networks for each age span and then to examine the age effects across these spans. Currently, we do not have sufficient samples for this purpose and will examine age effects in the future once the samples are available. Finally, the local functional homogeneity exhibited a significant correlation with the surface area, which indicates the structural basis of the local functional homogeneity, contributing to the inter-individual variability of the local functional homogeneity and of the functional covariance networks. Regarding the small percentage (<12 %) of variability of 2dReHo explained by the cortical morphology, we thus believe that the functional aspect of 2dReHo primarily drives the FCN findings. In the future, to achieve insights regarding the patterns of surface area variation across subjects, a more sophisticated investigation (e.g., regressing out the surface

area in the construction model of the FCNs) of this structure–function relation is warranted.

Conclusions

We observed remarkable regional variation, functional covariance and morphological association of local functional homogeneity across the cortical mantle. Our findings assign 2dReHo possible biological significance as a functional measure of regional segregation and integration of information processing regarding its cognitive and neurodevelopmental aspects.

Acknowledgments The authors would like to thank Drs. Olaf Sporns, Michael Peter Milham, Yu-Feng Zang and Hui-Jie Li for comments on an early version of the manuscript. All authors declare no competing financial interests. This work is partially supported by the National Key Technologies R&D Program of China (No. 2012BAI36B01), the Startup Foundation for Young Talents of Institute of Psychology (Y1CX222005, LJ), the Hundred Talents Program and the Key Research Program (KSZD-EW-TZ-002, XNZ) of Chinese Academy of Sciences, the Major Joint Fund for International Cooperation and Exchange of the National Natural Science Foundation (81220108014, XNZ) and others from Natural Science Foundation of China (11204369, 81270023, 81171409). Data were provided [in part] by the HCP WU-Minn Consortium, which is funded by the 16 NIH institutes and centers that support the NIH Blueprint for Neuroscience Research 1U54MH091657 (PIs: David Van Essen and Kamil Ugurbil), the McDonnell Center for Systems Neuroscience at Washington University.

References

- Aleman-Gomez Y, Janssen J, Schnack H, Balaban E, Pina-Camacho L, Alfaro-Almagro F, Castro-Fornieles J, Otero S, Baeza I, Moreno D, Bargallo N, Parellada M, Arango C, Desco M (2013) The human cerebral cortex flattens during adolescence. *J Neurosci* 33:15004–15010
- Alexander-Bloch A, Giedd JN (2013) Imaging structural co-variance between human brain regions. *Nat Rev Neurosci* 14:322–336
- Alexander-Bloch A, Raznahan A, Bullmore E, Giedd J (2013) The convergence of maturational change and structural covariance in human cortical networks. *J Neurosci* 33:2889–2899
- Amaral LA, Scala A, Barthelemy M, Stanley HE (2000) Classes of small-world networks. *Proc Natl Acad Sci USA* 97:11149–11152
- Amodio DM, Frith CD (2006) Meeting of minds: the medial frontal cortex and social cognition. *Nat Rev Neurosci* 7:268–277
- Andrews-Hanna JR, Smallwood J, Spreng RN (2014) The default network and self-generated thought: component processes, dynamic control, and clinical relevance. *Ann N Y Acad Sci* 1316:29–52
- Badre D (2008) Cognitive control, hierarchy, and the rostro-caudal organization of the frontal lobes. *Trends Cogn Sci* 12:193–200
- Badre D, D’Esposito M (2007) Functional magnetic resonance imaging evidence for a hierarchical organization of the prefrontal cortex. *J Cogn Neurosci* 19:2082–2099
- Badre D, D’Esposito M (2009) Is the rostro-caudal axis of the frontal lobe hierarchical? *Nat Rev Neurosci* 10:659–669
- Bassett DS, Bullmore E (2006) Small-world brain networks. *Neuroscientist* 12:512–523
- Bellec P, Rosa-Neto P, Lyttelton OC, Benali H, Evans AC (2010) Multi-level bootstrap analysis of stable clusters in resting-state fMRI. *Neuroimage* 51:1126–1139
- Bernhardt BC, Klimecki OM, Leiberg S, Singer T (2013) Structural covariance networks of the dorsal anterior insula predict females’ individual differences in empathic responding. *Cereb Cortex*. doi:10.1093/cercor/bht1072
- Biswal B, Yetkin FZ, Haughton VM, Hyde JS (1995) Functional connectivity in the motor cortex of resting human brain using echo-planar MRI. *Magn Reson Med* 34:537–541
- Biswal BB, Mennes M, Zuo XN, Gohel S, Kelly C, Smith SM, Beckmann CF, Adelstein JS, Buckner RL, Colcombe S, Dogonowski AM, Ernst M, Fair D, Hampson M, Hoptman MJ, Hyde JS, Kiviniemi VJ, Kötter R, Li SJ, Lin CP, Lowe MJ, Mackay C, Madden DJ, Madsen KH, Margulies DS, Mayberg HS, McMahon K, Monk CS, Mostofsky SH, Nagel BJ, Pekar JJ, Peltier SJ, Petersen SE, Riedel V, Rombouts SA, Rypma B, Schlaggar BL, Schmidt S, Seidler RD, Siegle GJ, Sorg C, Teng GJ, Veijola J, Villringer A, Walter M, Wang L, Weng XC, Whitfield-Gabrieli S, Williamson P, Windischberger C, Zang YF, Zhang HY, Castellanos FX, Milham MP (2010) Toward discovery science of human brain function. *Proc Natl Acad Sci USA* 107:4734–4739
- Blackmon K, Halgren E, Barr WB, Carlson C, Devinsky O, DuBois J, Quinn BT, French J, Kuzniecky R, Thesen T (2011) Individual differences in verbal abilities associated with regional blurring of the left gray and white matter boundary. *J Neurosci* 31:15257–15263
- Blondel VD, Guillaume GL, Lambiotte R, Lefebvre E (2008) Fast unfolding of communities in large networks. *J Stat Mech* P10008
- Blumensath T, Jbabdi S, Glasser MF, Van Essen DC, Ugurbil K, Behrens TE, Smith SM (2013) Spatially constrained hierarchical parcellation of the brain with resting-state fMRI. *NeuroImage* 76:313–324
- Breakspear M, Jirsa V, Deco G (2010) Computational models of the brain: from structure to function. *Neuroimage* 52:727–730
- Buckner RL, Sepulcre J, Talukdar T, Krienen FM, Liu H, Hedden T, Andrews-Hanna JR, Sperling RA, Johnson KA (2009) Cortical hubs revealed by intrinsic functional connectivity: mapping, assessment of stability, and relation to Alzheimer’s disease. *J Neurosci* 29:1860–1873
- Bullmore E, Sporns O (2009) Complex brain networks: graph theoretical analysis of structural and functional systems. *Nat Rev Neurosci* 10:186–198
- Bullmore E, Sporns O (2012) The economy of brain network organization. *Nat Rev Neurosci* 13:336–349
- Cabral J, Hugues E, Sporns O, Deco G (2011) Role of local network oscillations in resting-state functional connectivity. *Neuroimage* 57:130–139
- Cao M, Wang JH, Dai ZJ, Cao XY, Jiang L, Fan FM, Song XW, Xia MR, Shu N, Dong Q, Milham MP, Castellanos FX, Zuo XN, He Y (2014) Topological organization of the human brain functional connectome across the lifespan. *Dev Cogn Neurosci* 7:76–93
- Cauda F, Geminiani G, D’Agata F, Sacco K, Duca S, Bagshaw AP, Cavanna AE (2010) Functional connectivity of the posteromedial cortex. *PLoS ONE* 5:e13107
- Cavanna AE, Trimble MR (2006) The precuneus: a review of its functional anatomy and behavioural correlates. *Brain* 129:564–583
- Cole MW, Reynolds JR, Power JD, Repovs G, Anticevic A, Braver TS (2013) Multi-task connectivity reveals flexible hubs for adaptive task control. *Nat Neurosci* 16:1348–1355
- Collin G, Sporns O, Mandl RC, van den Heuvel MP (2013) Structural and functional aspects relating to cost and benefit of rich club

- organization in the human cerebral cortex. *Cereb Cortex*. doi:10.1093/cercor/bht064
- Cox RW (2012) AFNI: what a long strange trip it's been. *Neuroimage* 62:743–747
- Craddock RC, James GA, Holtzheimer PE, Hu XP, Mayberg HS (2012) A whole brain fMRI atlas generated via spatially constrained spectral clustering. *Hum Brain Mapp* 33:1914–1928
- Craddock RC, Jbabdi S, Yan CG, Vogelstein JT, Castellanos FX, Di Martino A, Kelly C, Heberlein K, Colcombe S, Milham MP (2013) Imaging human connectomes at the macroscale. *Nat Methods* 10:524–539
- Dale AM, Fischl B, Sereno MI (1999) Cortical surface-based analysis. I. Segmentation and surface reconstruction. *Neuroimage* 9:179–194
- Deco G, Jirsa VK (2012) Ongoing cortical activity at rest: criticality, metastability, and ghost attractors. *J Neurosci* 32:3366–3375
- Deco G, Jirsa V, McIntosh A, Sporns O, Kötter R (2009) Key role of coupling, delay, and noise in resting brain fluctuations. *Proc Natl Acad Sci USA* 106:10302–10307
- Deco G, Jirsa VK, McIntosh AR (2010) Emerging concepts for the dynamical organization of resting-state activity in the brain. *Nat Rev Neurosci* 12:43–56
- Deco G, Jirsa VK, McIntosh AR (2013) Resting brains never rest: computational insights into potential cognitive architectures. *Trends Neurosci* 36:268–274
- Destrieux C, Fischl B, Dale A, Hagren E (2010) Automatic parcellation of human cortical gyri and sulci using standard anatomical nomenclature. *Neuroimage* 53:1–15
- Dierker DL, Feczko E, Pruett JR Jr, Petersen SE, Schlaggar BL, Constantino JN, Harwell JW, Coalson TS, Van Essen DC (2013) Analysis of cortical shape in children with simplex autism. *Cereb Cortex*. doi:10.1093/cercor/bht294
- Eilers PH, Goeman JJ (2004) Enhancing scatter plots with smoothed densities. *Bioinformatics* 20:623–628
- Elton A, Gao W (2014) Divergent task-dependent functional connectivity of executive control and salience networks. *Cortex* 51:56–66
- Essen DC, Smith SM, Barch DM, Behrens TE, Yacoub E, Ugurbil K, Consortium WU-MH (2013) The WU-Minn human connectome project: an overview. *Neuroimage* 80:62–79
- Feinberg DA, Moeller S, Smith SM, Auerbach E, Ramanna S, Gunther M, Glasser MF, Miller KL, Ugurbil K, Yacoub E (2010) Multiplexed echo planar imaging for sub-second whole brain fMRI and fast diffusion imaging. *PLoS ONE* 5:e15710
- Fischl B (2012) FreeSurfer. *Neuroimage* 62:774–781
- Fischl B, Dale AM (2000) Measuring the thickness of the human cerebral cortex from magnetic resonance images. *Proc Natl Acad Sci USA* 97:11050–11055
- Fischl B, Sereno MI, Dale AM (1999) Cortical surface-based analysis. II. Inflation, flattening, and a surface-based coordinate system. *Neuroimage* 9:195–207
- Fjell AM, Westlye LT, Amlie I, Tamnes CK, Grydeland H, Engvig A, Espeseth T, Reinvang I, Lundervold AJ, Lundervold A, Walhovd KB (2013) High-expanding cortical regions in human development and evolution are related to higher intellectual abilities. *Cereb Cortex*. doi:10.1093/cercor/bht201
- Fox MD, Snyder AZ, Vincent JL, Corbetta M, Van Essen DC, Raichle ME (2005) The human brain is intrinsically organized into dynamic, anticorrelated functional networks. *Proc Natl Acad Sci USA* 102:9673–9678
- Frye RE, Liederman J, Malmberg B, McLean J, Strickland D, Beauchamp MS (2010) Surface area accounts for the relation of gray matter volume to reading-related skills and history of dyslexia. *Cereb Cortex* 20:2625–2635
- Gallos LK, Makse HA, Sigman M (2012) A small world of weak ties provides optimal global integration of self-similar modules in functional brain networks. *Proc Natl Acad Sci USA* 109:2825–2830
- Garrett DD, Samanez-Larkin GR, MacDonald SW, Lindenberger U, McIntosh AR, Grady CL (2013) Moment-to-moment brain signal variability: a next frontier in human brain mapping? *Neurosci Biobehav Rev* 37:610–624
- Glasser MF, Van Essen DC (2011) Mapping human cortical areas in vivo based on myelin content as revealed by T1- and T2-weighted MRI. *J Neurosci* 31:11597–11616
- Glasser MF, Sotiropoulos SN, Wilson JA, Coalson TS, Fischl B, Andersson JL, Xu J, Jbabdi S, Webster M, Polimeni JR, Van Essen DC, Jenkinson M, Consortium WU-MH (2013) The minimal preprocessing pipelines for the Human Connectome Project. *Neuroimage* 80:105–124
- Gogtay N, Giedd JN, Lusk L, Hayashi KM, Greenstein D, Vaituzis AC, Nugent TF, Herman DH, Clasen LS, Toga AW (2004) Dynamic mapping of human cortical development during childhood through early adulthood. *Proc Natl Acad Sci USA* 101:8174–8179
- Greve DN, Fischl B (2009) Accurate and robust brain image alignment using boundary-based registration. *NeuroImage* 48:63–72
- Griffanti L, Salimi-Khorshidi G, Beckmann CF, Auerbach EJ, Douaud G, Sexton CE, Zsoldos E, Ebmeier KP, Filippini N, Mackay CE, Moeller S, Xu J, Yacoub E, Baselli G, Ugurbil K, Miller KL, Smith SM (2014) ICA-based artefact removal and accelerated fMRI acquisition for improved Resting State Network imaging. *Neuroimage* 95C:232–247
- Grubbs FE (1969) Procedures for detecting outlying observations in samples. *Technometrics* 11:1–21
- Hagmann P, Cammoun L, Gigandet X, Meuli R, Honey CJ, Wedeen VJ, Sporns O (2008) Mapping the structural core of human cerebral cortex. *PLoS Biol* 6:e159
- Han X, Jovicich J, Salat D, van der Kouwe A, Quinn B, Czanner S, Busa E, Pacheco J, Albert M, Killiany R (2006) Reliability of MRI-derived measurements of human cerebral cortical thickness: the effects of field strength, scanner upgrade and manufacturer. *Neuroimage* 32:180–194
- Hayasaka S, Laurienti PJ (2010) Comparison of characteristics between region- and voxel-based network analyses in resting-state fMRI data. *NeuroImage* 50:499–508
- He Y, Wang L, Zang Y, Tian L, Zhang X, Li K, Jiang T (2007a) Regional coherence changes in the early stages of Alzheimer's disease: a combined structural and resting-state functional MRI study. *Neuroimage* 35:488–500
- He Y, Chen ZJ, Evans AC (2007b) Small-world anatomical networks in the human brain revealed by cortical thickness from MRI. *Cereb Cortex* 17:2407–2419
- He Y, Wang J, Wang L, Chen ZJ, Yan C, Yang H, Tang H, Zhu C, Gong Q, Zang Y, Evans AC (2009) Uncovering intrinsic modular organization of spontaneous brain activity in humans. *PLoS ONE* 4:e5226
- Hogstrom LJ, Westlye LT, Walhovd KB, Fjell AM (2013) The structure of the cerebral cortex across adult life: age-related patterns of surface area, thickness, and gyrification. *Cereb Cortex* 23:2521–2530
- Honey C, Sporns O, Cammoun L, Gigandet X, Thiran JP, Meuli R, Hagmann P (2009) Predicting human resting-state functional connectivity from structural connectivity. *Proc Natl Acad Sci USA* 106:2035–2040
- Hutchison RM, Everling S (2013) Broad intrinsic functional connectivity boundaries of the macaque prefrontal cortex. *Neuroimage* 88:202–211
- Im K, Pienaar R, Paldino MJ, Gaab N, Galaburda AM, Grant PE (2013) Quantification and discrimination of abnormal sulcal patterns in polymicrogyria. *Cereb Cortex* 23:3007–3015

- Jenkinson M, Beckmann CF, Behrens TE, Woolrich MW, Smith SM (2012) FSL. *Neuroimage* 62:782–790
- Kanai R, Rees G (2011) The structural basis of inter-individual differences in human behaviour and cognition. *Nat Rev Neurosci* 12:231–242
- Kelly C, Biswal BB, Craddock RC, Castellanos FX, Milham MP (2012) Characterizing variation in the functional connectome: promise and pitfalls. *Trends Cogn Sci* 16:181–188
- Kippenhan JS, Olsen RK, Mervis CB, Morris CA, Kohn P, Meyer-Lindenberg A, Berman KF (2005) Genetic contributions to human gyrification: sulcal morphometry in Williams syndrome. *J Neurosci* 25:7840–7846
- Lee JK, Lee JM, Kim JS, Kim IY, Evans AC, Kim SI (2006) A novel quantitative cross-validation of different cortical surface reconstruction algorithms using MRI phantom. *Neuroimage* 31:572–584
- Leech R, Sharp DJ (2014) The role of the posterior cingulate cortex in cognition and disease. *Brain* 137:12–32
- Levitt JG, Blanton RE, Smalley S, Thompson PM, Guthrie D, McCracken JT, Sadoun T, Heinichen L, Toga AW (2003) Cortical sulcal maps in autism. *Cereb Cortex* 13:728–735
- Li S, Han Y, Wang D, Yang H, Fan Y, Lv Y, Tang H, Gong Q, Zang Y, He Y (2010) Mapping surface variability of the central sulcus in musicians. *Cereb Cortex* 20:25–33
- Li X, Pu F, Fan Y, Niu H, Li S, Li D (2013) Age-related changes in brain structural covariance networks. *Front Hum Neurosci* 7:98
- Li G, Wang L, Shi F, Lyall AE, Lin W, Gilmore JH, Shen D (2014) Mapping longitudinal development of local cortical gyrification in infants from birth to 2 years of age. *J Neurosci* 34:4228–4238
- Liao W, Zhang Z, Mantini D, Xu Q, Wang Z, Chen G, Jiao Q, Zang YF, Lu G (2013) Relationship between large-scale functional and structural covariance networks in idiopathic generalized epilepsy. *Brain Connect* 3:240–254
- Lichtman JW, Denk W (2011) The big and the small: challenges of imaging the brain circuits. *Science* 334:618–623
- Long XY, Zuo XN, Kiviniemi V, Yang Y, Zou QH, Zhu CZ, Jiang TZ, Yang H, Gong QY, Wang L, Li KC, Xie S, Zang YF (2008) Default mode network as revealed with multiple methods for resting-state functional MRI analysis. *J Neurosci Methods* 171:349–355
- Luckmann HC, Jacobs HI, Sack AT (2014) The cross-functional role of frontoparietal regions in cognition: internal attention as the overarching mechanism. *Prog Neurobiol* 116:66–86
- Lyall AE, Shi F, Geng X, Woolson S, Li G, Wang L, Hamer RM, Shen D, Gilmore JH (2014) Dynamic development of regional cortical thickness and surface area in early childhood. *Cereb Cortex*. doi:10.1093/cercor/bhu027
- MacDonald SW, Nyberg L, Bäckman L (2006) Intra-individual variability in behavior: links to brain structure, neurotransmission and neuronal activity. *Trends Neurosci* 29:474–480
- Makris N, Kaiser J, Haselgrove C, Seidman LJ, Biederman J (2006) Human cerebral cortex: a system for the integration of volume- and surface-based representations. *Neuroimage* 33:139–153
- Margulies DS, Vincent JL, Kelly C, Lohmann G, Uddin LQ, Biswal BB, Villringer A, Castellanos FX, Milham MP, Petrides M (2009) Precuneus shares intrinsic functional architecture in humans and monkeys. *Proc Natl Acad Sci USA* 106:20069–20074
- McIntosh AR (2000) Towards a network theory of cognition. *Neural Netw* 13:861–870
- McKay DR, Kochunov P, Cykowski MD, Kent JW, Laird AR, Lancaster JL, Blangero J, Glahn DC, Fox PT (2013) Sulcal depth-position profile Is a genetically mediated neuroscientific trait: description and characterization in the central sulcus. *J Neurosci* 33:15618–15625
- Mechelli A, Friston KJ, Frackowiak RS, Price CJ (2005) Structural covariance in the human cortex. *J Neurosci* 25:8303–8310
- Milham MP (2012) Open neuroscience solutions for the connectome-wide association era. *Neuron* 73:214–218
- Miller EK (2000) The prefrontal cortex and cognitive control. *Nat Rev Neurosci* 1:59–65
- Moeller S, Yacoub E, Olman CA, Auerbach E, Strupp J, Harel N, Ugurbil K (2010) Multiband multislice GE-EPI at 7 tesla, with 16-fold acceleration using partial parallel imaging with application to high spatial and temporal whole-brain fMRI. *Magn Reson Med* 63:1144–1153
- Montembeault M, Joubert S, Doyon J, Carrier J, Gagnon JF, Monchi O, Lungu O, Belleville S, Brambati SM (2012) The impact of aging on gray matter structural covariance networks. *NeuroImage* 63:754–759
- Mueller S, Wang D, Fox MD, Yeo B, Sepulcre J, Sabuncu MR, Shafee R, Lu J, Liu H (2013) Individual variability in functional connectivity architecture of the human brain. *Neuron* 77:586–595
- Nakagawa TT, Jirsa VK, Spiegler A, McIntosh AR, Deco G (2013) Bottom up modeling of the connectome: linking structure and function in the resting brain and their changes in aging. *NeuroImage* 80:318–329
- Nooner KB, Colcombe SJ, Tobe RH, Mennes M, Benedict MM, Moreno AL, Panek LJ, Brown S, Zavitz ST, Li Q, Sikka S, Gutman D, Bangaru S, Schlachter RT, Kamiel SM, Anwar AR, Hinz CM, Kaplan MS, Rachlin AB, Adelsberg S, Cheung B, Khanuja R, Yan C, Craddock CC, Calhoun V, Courtney W, King M, Wood D, Cox CL, Kelly AM, Di Martino A, Petkova E, Reiss PT, Duan N, Thomsen D, Biswal B, Coffey B, Hoptman MJ, Javitt DC, Pomara N, Sidtis JJ, Koplewicz HS, Castellanos FX, Leventhal BL, Milham MP (2012) The NKI-Rockland sample: a model for accelerating the pace of discovery science in psychiatry. *Front Neurosci* 6:152
- Nordahl CW, Dierker D, Mostafavi I, Schumann CM, Rivera SM, Amaral DG, Van Essen DC (2007) Cortical folding abnormalities in autism revealed by surface-based morphometry. *J Neurosci* 27:11725–11735
- Panizzon MS, Fennema-Notestine C, Eyer LT, Jernigan TL, Prom-Wormley E, Neale M, Jacobson K, Lyons MJ, Grant MD, Franz CE, Xian H, Tsuang M, Fischl B, Seidman L, Dale A, Kremen WS (2009) Distinct genetic influences on cortical surface area and cortical thickness. *Cereb Cortex* 19:2728–2735
- Patriat R, Molloy EK, Meier TB, Kirk GR, Nair VA, Meyerand ME, Prabhakaran V, Birn RM (2013) The effect of resting condition on resting-state fMRI reliability and consistency: a comparison between resting with eyes open, closed, and fixated. *NeuroImage* 78:463–473
- Pienaar R, Fischl B, Caviness V, Makris N, Grant PE (2008) A methodology for analyzing curvature in the developing brain from preterm to adult. *Int J Imag Syst Tech* 18:42–68
- Power JD, Cohen AL, Nelson SM, Wig GS, Barnes KA, Church JA, Vogel AC, Laumann TO, Miezin FM, Schlaggar BL, Petersen SE (2011) Functional network organization of the human brain. *Neuron* 72:665–678
- Power JD, Barnes KA, Snyder AZ, Schlaggar BL, Petersen SE (2012) Spurious but systematic correlations in functional connectivity MRI networks arise from subject motion. *Neuroimage* 59:2142–2154
- Raichle ME, MacLeod AM, Snyder AZ, Powers WJ, Gusnard DA, Shulman GL (2001) A default mode of brain function. *Proc Natl Acad Sci USA* 98:676–682
- Rettmann ME, Kraut MA, Prince JL, Resnick SM (2006) Cross-sectional and longitudinal analyses of anatomical sulcal changes associated with aging. *Cereb Cortex* 16:1584–1594
- Rosner B (1983) Percentage points for a generalized ESD may-outlier procedure. *Technometrics* 25:165–172
- Rubinov M, Sporns O (2010) Complex network measures of brain connectivity: uses and interpretations. *Neuroimage* 52:1059–1069

- Saad ZS, Gotts SJ, Murphy K, Chen G, Jo HJ, Martin A, Cox RW (2012) Trouble at rest: how correlation patterns and group differences become distorted after global signal regression. *Brain Connect* 2(1):25–32
- Salimi-Khorshidi G, Douaud G, Beckmann CF, Glasser MF, Griffanti L, Smith SM (2014) Automatic denoising of functional MRI data: combining independent component analysis and hierarchical fusion of classifiers. *Neuroimage* 90:449–468
- Satterthwaite TD, Elliott MA, Gerraty RT, Ruparel K, Loughhead J, Calkins ME, Eickhoff SB, Hakonarson H, Gur RC, Gur RE, Wolf DH (2013) An improved framework for confound regression and filtering for control of motion artifact in the preprocessing of resting-state functional connectivity data. *Neuroimage* 64:240–256
- Schaer M, Cuadra MB, Tamarit L, Lazeyras F, Eliez S, Thiran J-P (2008) A surface-based approach to quantify local cortical gyrification. *IEEE Trans Med Imaging* 27:161–170
- Schnack HG, van Haren NE, Brouwer RM, Evans A, Durston S, Boomsma DI, Kahn RS, Hulshoff Pol HE (2014) Changes in thickness and surface area of the human cortex and their relationship with intelligence. *Cereb Cortex*. doi:10.1093/cercor/bht357
- Segonne F, Dale AM, Busa E, Glessner M, Salat D, Hahn HK, Fischl B (2004) A hybrid approach to the skull stripping problem in MRI. *Neuroimage* 22:1060–1075
- Segonne F, Pacheco J, Fischl B (2007) Geometrically accurate topology-correction of cortical surfaces using nonseparating loops. *IEEE Trans Med Imaging* 26:518–529
- Sepulcre J, Liu H, Talukdar T, Martincorena I, Yeo BT, Buckner RL (2010) The organization of local and distant functional connectivity in the human brain. *PLoS Comput Biol* 6:e1000808
- Smith SM, Beckmann CF, Andersson J, Auerbach EJ, Bijsterbosch J, Douaud G, Duff E, Feinberg DA, Griffanti L, Harms MP, Kelly M, Laumann T, Miller KL, Moeller S, Petersen S, Power J, Salimi-Khorshidi G, Snyder AZ, Vu AT, Woolrich MW, Xu J, Yacoub E, Uğurbil K, Van Essen DC, Glasser MF, WU-Minn HCP Consortium (2013) Resting-state fMRI in the Human Connectome Project. *Neuroimage* 80:144–168
- Sporns O (2013) The human connectome: origins and challenges. *NeuroImage* 80:53–61
- Sporns O, Tononi G, Edelman GM (2000) Theoretical neuroanatomy: relating anatomical and functional connectivity in graphs and cortical connection matrices. *Cereb Cortex* 10:127–141
- Sporns O, Tononi G, Kötter R (2005) The human connectome: a structural description of the human brain. *PLoS Comput Biol* 1:245–251
- Spreng RN, Sepulcre J, Turner GR, Stevens WD, Schacter DL (2013) Intrinsic architecture underlying the relations among the default, dorsal attention, and frontoparietal control networks of the human brain. *J Cogn Neurosci* 25:74–86
- Tian L, Ren J, Zang Y (2012) Regional homogeneity of resting state fMRI signals predicts Stop signal task performance. *Neuroimage* 60:539–544
- Tomasi D, Volkow ND (2010) Functional connectivity density mapping. *Proc Natl Acad Sci USA* 107:9885–9890
- Tononi G, Sporns O (2003) Measuring information integration. *BMC Neurosci* 4:31
- Tononi G, Sporns O, Edelman GM (1994) A measure for brain complexity: relating functional segregation and integration in the nervous system. *Proc Natl Acad Sci USA* 91:5033–5037
- Ungerleider LG, Haxby JV (1994) ‘What’ and ‘where’ in the human brain. *Curr Opin Neurobiol* 4:157–165
- van den Heuvel MP, Sporns O (2011) Rich-club organization of the human connectome. *J Neurosci* 31:15775–15786
- van den Heuvel MP, Kahn RS, Goñi J, Sporns O (2012) High-cost, high-capacity backbone for global brain communication. *Proc Natl Acad Sci USA* 109:11372–11377
- Van Essen DC, Dierker DL (2007) Surface-based and probabilistic atlases of primate cerebral cortex. *Neuron* 56:209–225
- Van Essen DC, Glasser MF, Dierker DL, Harwell J, Coalson T (2012) Parcellations and hemispheric asymmetries of human cerebral cortex analyzed on surface-based atlases. *Cereb Cortex* 22:2241–2262
- Van Horn JD, Grafton ST, Miller MB (2008) Individual variability in brain activity: a nuisance or an opportunity? *Brain Imaging Behav* 2:327–334
- Vuoksima E, Panizzon MS, Chen CH, Fiecas M, Eyler LT, Fennema-Notestine C, Hagler DJ, Fischl B, Franz CE, Jak A, Lyons MJ, Neale MC, Rinker DA, Thompson WK, Tsuang MT, Dale AM, Kremen WS (2014) The genetic association between neocortical volume and general cognitive ability is driven by global surface area rather than thickness. *Cereb Cortex*. doi:10.1093/cercor/bhu018
- Wang T, Chen Z, Zhao G, Hitchman G, Liu C, Zhao X, Liu Y, Chen A (2014) Linking inter-individual differences in the conflict adaptation effect to spontaneous brain activity. *Neuroimage* 90:146–152
- Wig GS, Laumann TO, Cohen AL, Power JD, Nelson SM, Glasser MF, Miezin FM, Snyder AZ, Schlaggar BL, Petersen SE (2013) Parcellating an individual subject’s cortical and subcortical brain structures using snowball sampling of resting-state correlations. *Cereb Cortex*. doi:10.1093/cercor/bht1056
- Wood JN, Grafman J (2003) Human prefrontal cortex: processing and representational perspectives. *Nat Rev Neurosci* 4:139–147
- Wright R, Kyriakopoulou V, Ledig C, Rutherford MA, Hajnal JV, Rueckert D, Aljabar P (2014) Automatic quantification of normal cortical folding patterns from fetal brain MRI. *Neuroimage* 91:21–32
- Xing XX, Zhou YL, Adelstein JS, Zuo XN (2011) PDE-based spatial smoothing: a practical demonstration of impacts on MRI brain extraction, tissue segmentation and registration. *Magn Reson Imag* 29:731–738
- Yan C, Gong G, Wang J, Wang D, Liu D, Zhu C, Chen ZJ, Evans A, Zang Y, He Y (2011) Sex- and brain size-related small-world structural cortical networks in young adults: a DTI tractography study. *Cereb Cortex* 21:449–458
- Yan CG, Cheung B, Kelly C, Colcombe S, Craddock RC, Martino AD, Li Q, Zuo XN, Castellanos FX, Milham MP (2013a) A comprehensive assessment of regional variation in the impact of head micromovements on functional connectomics. *NeuroImage* 76:183–201
- Yan CG, Craddock RC, Zuo XN, Zang YF, Milham MP (2013b) Standardizing the intrinsic brain: towards robust measurement of inter-individual variation in 1000 functional connectomes. *Neuroimage* 80:246–262
- Yang Z, Chang C, Xu T, Jiang L, Handwerker DA, Castellanos FX, Milham MP, Bandettini PA, Zuo XN (2014) Connectivity trajectory across lifespan differentiates the precuneus from the default network. *Neuroimage* 89:45–56
- Yeo BTT, Krienen FM, Sepulcre J, Sabuncu MR, Lashkari D, Hollinshead M, Roffman JL, Smoller JW, Zöllei L, Polimeni JR (2011) The organization of the human cerebral cortex estimated by intrinsic functional connectivity. *J Neurophysiol* 106:1125–1165
- Zang Y, Jiang T, Lu Y, He Y, Tian L (2004) Regional homogeneity approach to fMRI data analysis. *Neuroimage* 22:394–400
- Zanto TP, Gazzaley A (2013) Fronto-parietal network: flexible hub of cognitive control. *Trends Cogn Sci* 17:602–603
- Zhang Z, Liao W, Zuo XN, Wang Z, Yuan C, Jiao Q, Chen H, Biswal BB, Lu G, Liu Y (2011) Resting-state brain organization revealed by functional covariance networks. *PLoS ONE* 6:e28817
- Zhang Y, Fan L, Zhang Y, Wang J, Zhu M, Zhang Y, Yu C, Jiang TZ (2014) Connectivity-based parcellation of the human postero-medial cortex. *Cereb Cortex* 24:719–727

- Zielinski BA, Gennatas ED, Zhou J, Seeley WW (2010) Network-level structural covariance in the developing brain. *Proc Natl Acad Sci USA* 107:18191–18196
- Zielinski BA, Anderson JS, Froehlich AL, Prigge MB, Nielsen JA, Cooperrider JR, Cariello AN, Fletcher PT, Alexander AL, Lange N (2012) scMRI reveals large-scale brain network abnormalities in autism. *PLoS ONE* 7:e49172
- Zuo XN, Xing XX (2011) Effects of non-local diffusion on structural MRI preprocessing and default network mapping: statistical comparisons with isotropic/anisotropic diffusion. *PLoS ONE* 6:e26703
- Zuo XN, Xing XX (2014) Test-retest reliabilities of resting-state fMRI measurements in human brain functional connectomics: a systems neuroscience perspective. *Neurosci Biobehav Rev*. doi:[10.1016/j.neubiorev.2014.05.009](https://doi.org/10.1016/j.neubiorev.2014.05.009)
- Zuo XN, Ehmke R, Mennes M, Imperati D, Castellanos FX, Sporns O, Milham MP (2012) Network centrality in the human functional connectome. *Cereb Cortex* 22:1862–1875
- Zuo XN, Xu T, Jiang L, Yang Z, Cao XY, He Y, Zang YF, Castellanos FX, Milham MP (2013) Toward reliable characterization of functional homogeneity in the human brain: preprocessing, scan duration, imaging resolution and computational space. *Neuroimage* 65:374–386